

2

AD-A262 301



OFFICE OF NAVAL RESEARCH

Contract N00014-91-J-1927

R&T Code 413v001

Technical Report No. 6

SCANNING TUNNELING MICROSCOPY, ATOMIC FORCE MICROSCOPY, AND RELATED TECHNIQUES

by

SHELLY SNYDER AND HENRY S. WHITE

Published in

JOURNAL OF ANALYTICAL CHEMISTRY

64, 116R, 1992

University of Minnesota  
Department of Chemical Engineering and Materials Science  
Minneapolis, MN 55455

March 20, 1993

Reproduction in whole or in part is permitted for any purpose of the United States Government.

This document has been approved for public release and sale; its distribution is unlimited.

DTIC  
ELECTE  
MAR 25 1993  
E D

93 01 20 003

93-06113



2108

# REPORT DOCUMENTATION PAGE

Form Approved  
OMB No. 0704-0188

Public reporting burden for this collection of information is estimated to average 30 minutes per response, including the time for reviewing instructions, gathering existing data needed, reviewing the collection of information, sending comments regarding this burden estimate or any other aspect of this collection of information, including suggestions for reducing this burden to Washington Headquarters Services, Directorate for Information Operations and Reports, 1215 Jefferson Davis Highway, Suite 1204, Arlington, VA 22202-4302, and to the Office of Management and Budget, Paperwork Reduction Project (0704-0188), Washington, DC 20503.

<b>1. AGENCY USE ONLY (Leave blank)</b>		<b>2. REPORT DATE</b> March 20, 1993	<b>3. REPORT TYPE AND DATES COVERED</b> Technical 6/30/92 - 3/31/93	
<b>4. TITLE AND SUBTITLE</b> SCANNING TUNNELING MICROSCOPY, ATOMIC FORCE MICROSCOPY, AND RELATED TECHNIQUES			<b>5. FUNDING NUMBERS</b> N00014-91-J-1927	
<b>6. AUTHOR(S)</b> SHELLY SNYDER AND HENRY S. WHITE				
<b>7. PERFORMING ORGANIZATION NAME(S) AND ADDRESS(ES)</b> Dept. of Chemical Engineering and Materials Science University of Minnesota			<b>8. PERFORMING ORGANIZATION REPORT NUMBER</b>  Technical Report No. 6	
<b>9. SPONSORING, MONITORING AGENCY NAME(S) AND ADDRESS(ES)</b> Office of Naval Research 800 North Quincy Street Arlington, VA 22217			<b>10. SPONSORING, MONITORING AGENCY REPORT NUMBER</b>	
<b>11. SUPPLEMENTARY NOTES</b>				
<b>12a. DISTRIBUTION AVAILABILITY STATEMENT</b>  Unclassified/Unlimited			<b>12b. DISTRIBUTION CODE</b>	
<b>13. ABSTRACT (Maximum 200 words)</b>  <p style="text-align: center;"><b>This manuscript reviews the literature concerning STM, AFM, and other scanned-probe microscopies from January 1 through December 15, 1991.</b></p>				
<b>14. SUBJECT TERMS</b>			<b>15. NUMBER OF PAGES</b> 19	
			<b>16. PRICE CODE</b>	
<b>17. SECURITY CLASSIFICATION OF REPORT</b> Unclassified		<b>18. SECURITY CLASSIFICATION OF THIS PAGE</b> UL	<b>19. SECURITY CLASSIFICATION OF ABSTRACT</b>	
		<b>20. LIMITATION OF ABSTRACT</b>		

Accession For	
NTIS CRA&I	<input checked="" type="checkbox"/>
DTIC TAB	<input type="checkbox"/>
Unannounced	<input type="checkbox"/>
Justification	
By	
Distribution/	
Availability Codes	
Dist	Avail and/or Special
A-1	20

Reprinted from *Analytical Chemistry Fundamental Reviews*, 1992, 64.  
 Copyright © 1992 by the American Chemical Society and reprinted by permission of the copyright owner.

# Scanning Tunneling Microscopy, Atomic Force Microscopy, and Related Techniques

Shelly R. Snyder and Henry S. White\*

*Department of Chemical Engineering and Materials Science, University of Minnesota, 151 Amundson Hall, 421 Washington Avenue SE, Minneapolis, Minnesota 55455*

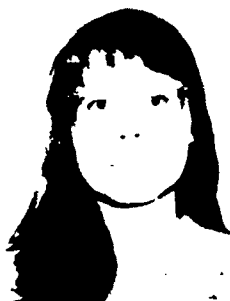
## INTRODUCTION

The last decade has seen the invention and development of scanning tunneling microscopy (STM) and atomic force microscopy (AFM). In 1986, the inventors of STM, Binnig and Rohrer (A1), received the Nobel Prize in Physics for their accomplishment. A nearly exponential increase in the number of publications describing applications of STM and AFM has occurred during the past few years. This remarkable growth is the best indication that these and related scanned-probe

techniques are being widely accepted as analytical tools for addressing fundamental issues in physics, chemistry, biology, and engineering.

This manuscript reviews the literature concerning STM, AFM, and other scanned-probe microscopies from January 1 through December 15, 1991. Recent reviews on Surface Characterization (A2) and Chemical Microscopy (A3), published in this journal, report on developments and applications of STM and AFM through the end of 1990. The literature

Shelly R. Snyder is completing her Ph.D. in Materials Science working with Professor Henry S. White at the University of Minnesota in the Department of Chemical Engineering and Materials Science. She received her B.S. degree in Chemistry from the University of Manitoba in 1987 and her M.S. degree in Materials Science from the University of Minnesota in 1990. Her thesis research is directed at probing the electronic and molecular structure of electroactive molecular adsorbates using scanning tunneling microscopy and tunneling spectroscopy. She is the 1991 recipient of the Edward G. Weston Summer Fellowship of the Electrochemical Society.



Henry S. White is Associate Professor in the Department of Chemical Engineering and Materials Science at the University of Minnesota. He received his B.S. degree in 1978 from the University of North Carolina, and his Ph.D. degree in 1983 from the University of Texas. He joined the faculty at the University of Minnesota in 1984 following a Postdoctoral Research Appointment at the Massachusetts Institute of Technology. He is a recipient of the Office of Naval Research Young Investigator Award in Chemistry and currently holds the Shell Chair of Chemical Engineering and Materials Science at the University of Minnesota. His research interests include electrochemistry and interfacial forces.



cited in this review is taken from a search of the STN International Database and Current contents. A significant number of citations are from the Proceedings of the Fifth International Conference on STM/Spectroscopy and the First International Conference on Nanometer Scale Science and Technology, published in the *Journal of Vacuum Science & Technology B*, Volume 9, 1991. This latter volume contains an excellent collection of research articles that are representative of current trends in the STM/AFM community.

STM is used throughout this review as an interchangeable abbreviation for both scanning tunneling microscopy and the scanning tunneling microscope. AFM is similarly used as an abbreviation for both the technique and the instrument.

## A. BOOKS AND REVIEWS

An extensive review of the theoretical and experimental aspects of STM is given by Chen (A4). The NATO ASI series book (A5), entitled *Scanning Tunneling Microscopy and Related Methods*, edited by Behm, Garcia, and Rohrer, discusses recent developments in the theory and applications of STM and AFM, as well as related optical and acoustic microscopies. This series addresses applications of STM in investigations of metal and semiconductor surfaces, organic and biological materials, and liquid-solid interfaces.

Much recent effort has been devoted to the design and characterization of probe tip. The effects of the electric field surrounding the tip is a fundamental issue in addressing surface damage frequently observed during imaging and in employing STM for intentional surface modifications. Binh and Garcia address these subjects in a review dealing with the role of STM tips in ion emission and surface melting (A6). The usefulness of the STM in its ability to manipulate atoms and molecules on a surface in a controlled fashion has been reviewed by Eng and Fuchs (A7).

Several review articles deal with specific applications of the STM. Gimzewski has considered the interpretation of the structural details observed in images of metals, molecules, and biological complexes in terms of electronic charge contours (A8). Metzger and Panetta reported on the use of STM for studying Langmuir-Blodgett films (A9). Lieber and Wu have extensively studied charge density waves in low-dimensional materials, such as tantalum dichalcogenides, and have reviewed the effects of metal substitution in these materials (A10). The electronic structure of small metallic particles and their interaction and modulation of the substrate electronic

structure is reviewed by Sattler (A11). Surface diffusion of metal atoms as observed by several microscopic techniques, including STM, has also been reviewed (A12).

The principles and operation of the electrochemical STM are discussed by Chidsey (A13). Shortcomings of this technique in the study of materials which are not atomically flat are discussed.

AFM, like STM, is capable of imaging surfaces with atomic resolution but can image both conductive and nonconductive samples. Developed by Binnig, Quate, and Gerber in 1986 (A14), the AFM has similar status and flexibility in usage as the STM. In AFM, a sharp tip is mounted on a microcantilever arm and rastered across the sample surface. In a typical configuration, the deflection of a light off the back of the cantilever is used to monitor the force applied by the cantilever on the sample. In systems of this type, forces as small as  $10^{-9}$  N are applied to the substrate, thereby reducing damage to the sample. A useful review of the subject highlights five cantilever drive systems and seven deflection detection systems (A15).

## B. INSTRUMENTATION AND PROBE TIPS

Several researchers describe home-built STM's (B1, B2) and novel coarse positioning devices (B3, B4). Various calibration methods (e.g., an inductive displacement transducer and Michelson interferometer) for the piezoelectric element, which controls the fine position of the tunneling tip, have been compared (B5). Sugawara et al. have combined the STM with the AFM for simultaneous imaging of the repulsive contact forces and surface conductance between a probe and sample and present data for graphite (B6).

STM's are now being integrated into multifunctional surface analysis instruments where a number of measurements or surface modifications can be performed on the sample without removal from the instrument. Some of the combinations include an optical microscope (B7), molecular-beam epitaxy system (B8), and IR reflection-adsorption spectrometer (B9).

Interest in ferromagnetic materials and superconductors has led, in part, to the development of a magnetic force microscope based on the STM. This instrument can simultaneously measure topography and magnetic forces between a flexible magnetic tip and the sample (B10, B11). Variations on this technology include STM's which can detect spin-polarized electrons and thus magnetic structures at the atomic scale (B12) or which can detect spatially resolved spin-polarized secondary electrons emitted from the sample with the STM operating in the field emission mode (B13).

Stoll and Gimzewski have compared atomically resolved images of Au(110)  $1 \times 2$  and Cu(111) using both the conventional and differential modes of STM (B14). The authors conclude that the differential mode, which is a phase-sensitive technique designed to reduce noise, results in an increase in the  $1/f$  component. Variations in the local conductivity and topography of copper samples have been simultaneously monitored by analysis of the high-frequency component of the tunneling current noise (B15). A scanning chemical potential microscope (SCPM) has been developed to measure thermoelectric potential variations related to atomic scale variations in the surface chemical potential gradient (B16). The thermoelectric voltage produced at the tunnel junction between a tip and sample, which is heated, is measured simultaneously with the STM current images. Kordic et al. have used a two-dimensional STM to image the interface between the p- and n-type regions of a biased Si p-n junction (B17).

Yau et al. (B18) have used a novel electric field effect to deposit gas-phase Al atoms in local regions directly beneath the STM tip. This technique allows for writing of nanometer-sized features on surfaces.

The STM current can be enhanced or controlled by photoexcitation of electronic transitions within the tunnel junction. Voelcker et al., for instance, have illuminated tunnel junctions with laser radiation during STM measurements (B19, B20). A dc current generated by rectifying the laser light, combined with a difference-frequency signal, is used to obtain atomically resolved images of graphite and to control the tip-to-sample separation. This system allows image acquisition without an external applied bias voltage, and may be suitable for the study of insulators. In order to study adsorbates at the STM interface, Grafstrom et al. irradiate the tunneling gap with two laser beams, one resonant with

the adsorbate, and suppress the thermal contribution to the tunneling current by modulating the amplitude of both beams with a 180° phase shift (B21). With this system, small changes in the tunneling current induced by resonant optical excitation of the adsorbate can be detected.

Several authors have described photon scanning tunneling microscopes (PSTM), in which the tunneling of photons from an evanescent wave originating at the substrate to a optical fiber tip is monitored (B22–B26). Jiang et al. have constructed a high-resolution PSTM (80-nm resolution) employing a AlGaAs diode laser (B27). PSTM can be operated to measure photon spectra, isochromat spectra, and angular photon distributions and to map local photon intensities. Photoassisted scanning tunneling spectroscopy (STS), based on illuminating a semiconductor substrate during imaging, has been used to study WSe<sub>2</sub> (B28), Si(111) and Si(001) (B29), n-type InP(100), p-type GaAs(100) (B30), Cu<sub>2</sub>Se<sub>2</sub> (B31), Al<sub>1-x</sub>Ga<sub>x</sub>As heterostructures (B32), and InAs<sub>2</sub>P<sub>1-x</sub>/InP quantum well structures (B33).

A comparison of several low-temperature STM's operating in liquid helium has been reported (B34). Giessibl et al. have constructed a UHV combined AFM/STM operating at 4.2 K (B35), and Cohen and Wolf have designed a microwave coupled cryogenic STM (B36). Variable-temperature STM's (B37) have been developed for investigating the substrate structure and electronic properties of superconductors (e.g., Pb films (B38)), organic conductors (e.g., TTF-TCNQ (B39)), and layered transition-metal dichalcogenides (e.g., 1T-TaS<sub>2</sub> (B40)).

Moeller et al. have used the thermal noise within the tunnel junction to operate an STM at zero bias between the sample and tip, thus allowing small differences in the potential (with a resolution of 1 μV) at various points on a polycrystalline Ag sample to be detected (B41). STM systems with potentiostatic/galvanostatic control of the sample and potentiostatic control of the STM tip have been reported (B42). (See also section F). Yuan et al. have proposed a new method for imaging nonconductive samples, such as biological complexes, which relies on the surface condensation of water molecules to provide a path for the electric current (which is carried by ions rather than electrons) (B43).

New advances in AFM instrumentation include a high-speed AFM (B44), a rocking beam electrostatic balance for measuring small forces (B45), an interferometer to measure the cantilever deflection (B46), high precision positioning stages, and an X-Y scanner whose displacement is controlled by a two-dimensional optical interferometer (B47) or by a two-dimensional optical beam displacement sensor (B48).

Techniques for measuring the surface photovoltage on semiconducting samples using attractive-mode AFM have been reported (B49, B50). The AFM potentiometer allows measurements to be made in air with a spatial resolution of a few tens of nanometers and a voltage resolution of less than 1 mV. Denk and Pohl have used the AFM to image the local electrical dissipation between the AFM probe and a layered GaAs/AlGaAs substrate by monitoring the mechanical Q during scanning (B51). Barrett and Quate have developed a scanning capacitance microscope based on the AFM which can simultaneously monitor the capacitance between a conducting tip and substrate and the film topography as a function of lateral position (B52). The AFM employed in the capacitive force sensing mode can be used to map the dopant profile in semiconductors. Limits in the sensitivity and resolution of the method are described by Abraham et al. (B53).

The probe tip remains a major concern in STM, tunneling spectroscopy, and AFM measurements. Characterization of the atomic arrangement and chemical composition of atoms at the tip remains important in understanding how these parameters affect images and spectroscopic data. A combination of the atom probe and field emission electron energy spectrometer have been used to characterize the atomic configuration of the tip apex (B54). X-ray photoelectron and Auger electron spectroscopies have been used to identify the primary surface contaminants on electrochemically etched tungsten STM tips as CO, graphite, WC, and tungsten oxide (B55).

Several unusual STM tips have been described during the past year. The tunneling characteristics and morphology of Mo tips covered by adsorbed Si atoms (B56) was reported. Venkateswaran et al. have reported staircase-shaped I-V

tunneling curves in a oxidized Si tip-graphite substrate junction, resulting from a Coulomb blockade effect in the oxide layer of the Si tip (B57). Ikebe et al. have discussed the interpretation of images of graphite when a corner of a ReO<sub>3</sub> single crystal is used as the tunneling tip in STM (B58).

The application of micromachined Si force sensors in AFM have been discussed (B59), as well as etching techniques for mass producing Si sensors (B60). Hellemans et al. imaged diamond tips and metallic tips in a tip-to-tip configuration in the AFM and discuss the roles of the tip and sample on the resulting images (B61). Drexler has proposed a class of AFM-like devices that would allow imaging of the same sample area with an array of molecular tips of atomically defined structure (MTA) (B62). MTA's could have various chemical binding sites which would enable local nanofabrication by specific chemical interactions with the surface.

### C. THEORY

Due to the relative novelty of STM and AFM as surface analytical tools, the vast majority of experimental reports consider, albeit at a qualitative level, fundamental issues related to producing image contrast. In both STM and AFM, the interaction of the probe tip with the surface are of paramount importance in image interpretation and in surface modifications and damage (see also section E). The recent literature cited below reflects these concerns. Questions continue to arise concerning the ability to obtain high-resolution images under conditions where strong physical and chemical forces may alter the tip and/or substrate structure.

Theoretical studies focused on relating the surface electronic charge distribution to the contrast observed in STM images continued from the 1980's; a larger percentage of this effort, however, is now focused on materials (solids and adsorbates) other than pyrolytic graphite, which dominated the attention of theorists for the past 5 years. Representative articles from this field are cited in the following discussion.

The STM tip has been modeled as a polyatomic crystalline surface where the total tunneling current is the sum of the currents from tip atoms to each substrate atom (C1). This model can account for superperiodic structures frequently observed in STM images. Using a first principles local density approximation method with the tunneling Hamiltonian formalism, the arrangement of atoms (e.g., W, Pt, C/W, and TiC clusters) at the tip apex has been shown to have a larger effect on the STM image than the chemical composition of the tip (C2). Tsukada et al. have also modeled the differences observed in STM images and STS curves for clusters (e.g., W<sub>10</sub>[110], W<sub>13</sub>[110], W<sub>14</sub>[110], and Pt<sub>10</sub>[111]) with different geometries (C3).

Landman and Luedtke have extensively studied the mechanics and dynamics of the tip-substrate interactions in STM and AFM (C4). Using large-scale molecular dynamics calculations, they simulated atomic scale events occurring during approach of a Au(001) tip to a Ni(001) substrate, the subsequent jump to point contact, and retraction of the tip from the substrate. Chen and Hamers have calculated the apparent barrier height, including tip-sample forces, in STM measurements and found agreement between calculated and experimental data (C5).

The role of the image potential in the absence and presence of surface states has been discussed by several authors (C6, C7). Methods have been discussed for determining the effective surface potential, based on measuring the differential conductance or on measuring the apparent barrier height at various tip-sample separations (C8). The effects of quantum states induced by the geometry of the tunneling barrier at small tip-to-sample distances has also been discussed (C9). Garcia has shown that negative resistance characteristics for a tip-vacuum-Ni(100) junction can occur due to the presence of localized surface barrier states (C10). Denk and Pohl have solved Laplace's equation for a metallic or dielectric tip-to-sample geometry and discuss the importance of electromagnetic fields and plasmons in inelastic tunneling and light emission during tunneling (C11).

Sass and Gimzewski have qualitatively discussed the applicability of the STM for studying electron transfer in solution at the metal-electrolyte interface and the role of solvent dynamics in the electron-exchange process (C12).

Ab initio quantum mechanical calculations have been used to interpret the contrast in STM images of MoS<sub>2</sub> and MoTe<sub>2</sub>

(C13). A two-band Peierls-Hubbard model was used to study the superlattice phases in halogen-bridged mixed-valence transition-metal linear MX chain complexes (C14). Using the Landauer formula for the tunneling current, good agreement between calculated and experimental STM images for benzene on Rh(111) has been obtained (C15). Joachim has also discussed the conductance of a single molecule in terms of through-bond tunneling and through-space tunneling (C16). The influence of small molecules such as water, ammonia, and methane on the energy of the highest-occupied electronic states of benzene, which are involved in the tunneling mechanism, has also been considered (C17).

Theoretical calculations of the  $\sqrt{3} \times \sqrt{3}$  Ag/Si(111) structure based on a honeycomb chained trimer model have been presented and compared to STM images (C18, C19). Kariotis and Lagally have modeled various terrace-edge properties such as the distribution of kink lengths and edge displacements on vicinal surfaces (C20). Molecular dynamics calculations were used to model the reconstruction of the Si(001) surface and determine the relative stabilities of the  $(2 \times 2)$  and  $(2 \times 1)$  dimers (C21). Self-consistent quantum chemistry cluster calculations were used to determine the effects of bias and surface defects on the appearance of the dimers in an STM image (C22). Tanaka and Tsukada have used Green's function method to obtain the local DOS in a superconductor-semiconductor-superconductor junction and have compared their results to experimental data (C23).

Interpretation of AFM images requires careful consideration of the surface forces (dispersion, electrostatic, etc.) between the tip and substrate. A general theory for AFM tip interactions in the contact force regime which relies on taking force derivatives along the surface to enhance the images has been described (C24). Girard and Bouju have used a self-consistent formalism to determine the dispersion equation of the coupled electromagnetic modes between a rough surface and dielectric tip and relate these results to AFM imaging (C25). van der Waals interaction forces between a metallic tip and nonplanar dielectric have been modeled and related to the AFM operating in the attractive mode (C26, C27). Various approximations used to relate the previously found dispersion relations to simpler models (i.e., continuum description, pairwise summation models, etc.) have also been proposed (C28). Hartman has modeled the van der Waals forces between the tip and sample in AFM, on the basis of macroscopic quantum field theory, and shows that the VDW forces reflect the surface dielectric properties. In addition, the presence of highly polar liquids in the gap has been shown to reduce the VDW forces, reducing the tendency for the tip to jump to contact with the substrate (C27).

Ducker et al. used the AFM to measure the force between a silica sphere attached to an AFM cantilever tip and a flat planar surface of NaCl and demonstrate that the forces are consistent with the double-layer theory of colloidal forces except at very short distances (C29). Krantzman et al. have compared calculated constant-force mode AFM images of the two cleavage planes of the (100) surface of D,L-leucine and find that they are virtually indistinguishable if the tip is modeled as a cluster (C30). In contrast, a distinction between the two surface planes may be made if one monitors the variation in topography as a function of force in different scans. *Ab initio* total-energy calculations of the interaction potential between graphite and Pd have been reported (C31). The atomic scale modulation of the friction force and the stick-slip motion at the interface of the Pd/graphite system in a friction force microscope is discussed (C32) and used to model the effects of long-range VDW forces on the tip-substrate interaction (C33). Forcada et al. have also employed a theoretical model of tip-substrate interactions in AFM to discuss discrepancies between the thickness of lubricant films as measured by AFM and ellipsometry (C34).

## D. INTERFACIAL STUDIES

**D.1. Metal Surfaces and Clusters.** STM is well suited for investigating the nucleation and growth of metal films on atomically flat metal and semiconductor substrates. A significant fraction of articles published during the last year focus on this area, with particular attention given to ultrahigh vacuum studies of well-defined substrates. Metal deposition on insulating substrates, such as polymer films, can be investigated using AFM but has not been as extensively re-

searched. The large body of literature describing STM and AFM investigations of metal films and clusters prohibits an extensive survey of the literature in this field; the following sections are intended to indicate current research activities and to demonstrate the capabilities of scanned-probed methods. The literature is organized by the nature of the substrate (i.e., metals, semiconductors, insulators, etc.). Specialized and related research areas, including surface reconstructions and ion-implanted surfaces, are reviewed below in separate sections.

**Metal Substrates.** Au single crystals are often chosen as a substrate for nucleation and growth studies due to the choice of several preparations that yield clean, atomically flat surfaces. Chambliss et al. studied the inhomogeneous aggregation and growth of Ag in the monolayer regime on Au(111) (D1). This same group found that Ni deposited on Au(111) nucleated in ordered islands commensurate with the  $\sqrt{3} \times 22$  reconstruction (D2, D3). In other studies, the deposition of submonolayer coverages of Fe on Au(111) yielded polygonal islands (fcc structure); however, at three monolayers, a transition to the bcc structure occurs (D4). The electrocrystallization of Cu on Au(111) was found to preferentially nucleate at defect sites and step edges (D5). Magnussen et al. investigated electrocrystallization of Cu on Au(111) and Au(100) and observed quasi-hexagonal and hexagonal adlayer lattices (D6).

Poetschke and Behm have studied the interfacial strain between Cu and Ru(0001) using STM. A structural transformation from the more tightly bound first Cu layer to a unidirectional contracted second Cu layer was observed (D7). Poetschke et al. also studied the deposition of Cu and Au films on Ru(0001) and found that differences existed in the two-dimensional growth of the metals (D8).

**Pyrolytic Graphite.** Metallic clusters have been studied extensively on highly oriented pyrolytic graphite (HOPG), which serves as a model substrate, having been well characterized by STM during the past decade. Schleicher et al. observed ~10-nm diameter Ag and C particles on HOPG and found that the particle surface concentration and shape differed from that expected based on TEM studies (D9). Tip-particle and/or particle-surface interactions were proposed to be the source of the observed discrepancies. The initial stages of Au film formation on HOPG was reported to occur by coalescence of microclusters, ~2-5 nm in diameter, into larger islands (D10). The preparation of ~5-nm Au particles on HOPG has also been discussed (D11). Womelsdorf et al. studied the effect of different aggregating agents on the deposition of Au colloidal suspensions on HOPG and found that ionic salts deposited with the gold formed an ordered hexagonal lattice (D12). Becker et al. found that Au<sub>55</sub> clusters deposited on HOPG are stabilized by chemical bonding of phosphine to the Au surface (D13). Au and Pd clusters deposited on HOPG and Au were studied by Van de Leemput et al. (D14) who imaged ligand-stabilized Au<sub>55</sub>(PPh<sub>3</sub>)<sub>12</sub>C<sub>16</sub> and Pd<sub>55</sub>(phen)<sub>12</sub>C<sub>20</sub>. Images of the clusters obtained with a cluster attached to the tip are also interpreted in terms of the tunnel distance. On a larger scale, Strong et al. studied Au thermally evaporated on HOPG and found the islands were approximately triangular- or diamond-shaped and composed of stacked layers of (111) planes (D15).

Kojima et al. reported on the deposition of 4-nm Pd clusters on HOPG which coalesced and grew epitaxially along the (111) direction (D16). Siperko studied a Pd-Sn catalyst adsorbed on the basal plane of HOPG and found that the catalyst particles formed an ordered array (D17). Subsequent electroless Cu deposition over the catalyst particles resulted in a uniform coating of Cu. Kennedy et al., using STM and AFM, investigated the nucleation and growth of a Pd colloid, followed by deposition of electroless Cu, on HOPG for optimizing the procedures used in manufacturing multilayer circuit boards (D18).

Yeung and Wolf studied Pt catalysts prepared by impregnation and ion exchange of the precursor salt solutions on HOPG (D19). The annealing of Pt thin films deposited on HOPG was investigated as a function of temperature (D20). Electronic surface perturbations of the HOPG lattice near Pt particles have been attributed to periodic charge density modulations (D21, D22).

**Semiconductor Substrates.** The atomic structure of semiconductor-metal interfaces dominates the electrical properties

of many microelectronic devices. Scanned probe methods are capable of resolving the atomic surface position of metal adatoms during the first stages of metal deposition, thus providing a means of obtaining detailed experimental correlations between structural and electronic properties. As expected, investigations of metal deposition on Ge, Si, and GaAs dominated the research activities in this area.

Bremer et al., using AFM, showed that vapor deposition of Cu on Ge substrates formed thin films by coalescence of small atomic aggregates of Cu atoms (D23). They also investigated the morphology and oxidation state of the film after exposure to ethylene oxide. Leibele et al. found that Sb films exhibit different morphologies when deposited on Ge(110) depending on the temperature during deposition (D24). Krausch et al. studied In films on Ge(100) at room temperature and found that, even in the submonolayer range, In island growth occurs in three dimensions and the films are rough up to several hundred monolayers (D25).

Yang et al. have studied the interface between thermally evaporated Ti on GaAs(110) (D26). These same authors have also examined Ag nucleation and growth on GaAs(110) at 300 K and have found Ag atoms nucleate with no preferential orientation on the substrate and grow into clusters of ~250 atoms (D27). Continued deposition results in the growth and coalescence of the clusters, with preferential orientation occurring at ~5 monolayers. Trafas et al. have studied the nucleation and growth of Cr overlayers on GaAs(110) (D28). Their studies indicated that the initial Cr adatom surface mobility is high due to weak chemisorption to the GaAs substrate and that adatoms show a preferential clustering in the [211] direction. Disorder in the clusters was attributed to intermixing of the Cr with Ga and As atoms. Phaner et al. have compared the morphological difference between Au vapor-deposited on n-GaAs and an autoactivated electrodeless Au film on the same n-GaAs sample (D29). Clustering of Al atoms deposited on p-GaAs(110), with preferential nucleation of Al over the Ga sites, has also been investigated (D30). The morphology of epitaxial fcc Co/Pd(111) superlattices grown on GaAs(110) was reported by England et al. (D31).

Bauher has used various techniques, including STM, to develop a structural model for the  $5 \times 1$  phase observed in the Au/Si(111) system at low coverages (D32). Hasegawa et al. have studied the initial stages of Au growth on Si(111) and found that, at low coverages, the Au-adsorbed  $5 \times 2$  structure does not interfere with the Si  $7 \times 7$  structure (D33). However, the Si substrate begins to show the  $5 \times 2$  structure with increasing Au coverage. Similarly for low coverages of Pb on Si(111)  $7 \times 7$ , the Pb atoms occupy sites above and between the Si adatoms leaving the  $7 \times 7$  structure intact. An unusual  $\sqrt{3} \times \sqrt{3}$  phase having a Si:Pb ratio of 1:1, appeared during annealing (D34). Nogami et al. investigated Al films deposited on Si and showed that Al forms rows of adsorbed dimers which are perpendicular to the Si dimer rows of the Si(100) surface (D35). As the coverage of Al is increased, local  $2 \times 3$  and  $2 \times 2$  phases develop, which then evolve into a  $2 \times 2$  array of dimers at ~0.5 monolayer. At larger surface coverages, Al clusters grow on the  $2 \times 2$  surface. Sahara et al. studied the growth of Al films photodeposited on Si wafers from dimethylaluminum hydride (DMAH). Their studies indicated that the morphology of the Al islands is independent of illumination, ruling out photoinduced migration of the Al adatoms (D36, D37). Hashizume et al. have studied the adsorption of alkali-metal ions, including Li, K, and Cs, on Si(111) and Si(100) by means of field-ion STM and find that the alkali-metal atoms are almost completely ionized on the Si(111)  $7 \times 7$  surface; a small charge transfer occurs on the Si(100)  $2 \times 1$  surface (D38-D41). An extensive set of total-energy and force calculations have been used to model the interaction of alkali metals on Si(001)  $2 \times 1$  at different surface coverages (D42).

Elswijk et al. have reported investigations of Sb deposits on Si and observed that, at low Sb coverages, the adatoms substitute for Si in the  $7 \times 7$  reconstruction of Si(111) (D43). At ~1/3 monolayers, the distorted  $7 \times 7$  structure as well as a  $\sqrt{3} \times \sqrt{3}$ -R30° reconstruction was observed while at full monolayer coverages, a  $1 \times 1$ ,  $2 \times 1$ , and a second  $\sqrt{3} \times \sqrt{3}$  reconstruction were observed. The electronic state density of clean Si  $7 \times 7$  was compared to these Sb lattices. Nogami et al. found that the surface was terminated in a symmetric Sb dimer structure and the Sb grows as additional layers of

dimers rather than substituting for the topmost layer of Si dimers (D44). An Sb dimer structure was also found on the Si(001)  $2 \times 1$  surface (D45, D46). Beski et al. have also studied the evolution of In-induced reconstructions on Si(100)  $2 \times 1$  as a function of temperature and In surface coverage (D47, D48).

Other metal deposits on semiconductors studied by STM include Cs on InSb(110) (D49) and GaAs(110) (D50), Mg on GaAs(110) (D51), Sm on GaAs(110) (D52), S on GaAs (D53), and Au on GaAs(110) (D54).

**Insulating Substrates.** Metal deposition on mica has been reported by numerous research groups (D55). Rabe and Buchholz observed that surface modification of Ag(111) films epitaxially grown on mica was caused by field evaporation of the sample or tip material and not by current effects (D56). Colchero et al. used AFM to study Pd clusters evaporated on mica in UHV (D57). The authors found that the truncated trigonal shape of the clusters had a diameter to height ratio of ~10, agreeing with TEM measurements. Buchholz et al. compared Au, Pd, and Cr films evaporated on mica at various substrate temperatures and found that epitaxially grown Ag(111) films evaporated at 275 °C exhibit the largest and flattest terraces (D58). dc sputtering, ion beam deposition, and thermal deposition of various metallic films have been compared using STM (D59).

Dawson et al. studied the surface roughness of Ag films deposited on glass and CaF<sub>2</sub> and compared these results to those obtained from surface-enhanced Raman spectroscopy (SERS) (D60). They suggest that the small SERS signals obtained on fast-deposited Ag films are the result of the small grain size, leading to an increase in the elastic scattering of surface-plasmon polaritons at the grain boundaries and subsequently to a decrease of the SERS signal. Yamada et al. prepared atomically flat Au films deposited on polyimide and SiO<sub>2</sub> using an ionized cluster beam and observed a correlation of the film surface roughness with acceleration voltages (D61). Similar studies of Au films deposited on silica by evaporation and ion-assisted deposition were reported (D62).

**Surface Reconstructions.** The reconstruction of single-crystal metal surfaces on exposure to various adsorbates, in particular oxygen, has been studied extensively by STM. Using AFM, Weisenborn et al. imaged the  $\sqrt{3} \times \sqrt{3}$ -R30° structure of Bi(111) in air (D63). Using STM, Meyer et al. found that the W(001) surface formed a two-domain  $2 \times 1$  structure after the oxygen covered surface was annealed at >1000 °C (D64). They also confirmed the missing-row model for the  $2 \times 1$  structure and showed the preferred location for the O atom was either over a 3-fold hollow site or over a W atom in the second layer.

Kopatzki and Behm discuss image contrast mechanisms for features observed on oxygen-covered Ni(100) surfaces (D65). Haase et al. investigated the missing-row reconstruction of the (110) terraces of Ni(771) when exposed to oxygen (D66). Baeumer et al. showed that Ni(100) exposed to O<sub>2</sub> forms a 4-5 layer thick film of NiO(100) comprised of 50-Å crystallites (D67). A large mismatch in the lattice constants of Ni and NiO causes strain between the metal and oxide layer and leads to defect sites between the NiO islands.

Besenbacher et al. studied various metal and semiconductor surfaces, including Cu, using STM and found similarities in the final oxygen-induced reconstructions of these materials; however, the growth modes were different (D68). Kern et al. studied the Cu(110)  $2 \times 1$  O surface and found that anisotropic Cu-O islands are arranged into periodic strips along the (001) direction (D69). The width between the strips was dependent on the oxygen coverage and temperature. Winterlin et al. studied the diffusion of Cu and O atoms in the reconstruction of Cu(110) and found that the rate-limiting step in the transformation of the  $1 \times 1$  to  $2 \times 1$  reconstruction was the diffusion of Cu atoms from stepped regions (D70). In addition, it was observed that linear Cu-O-Cu strings stabilize the growth of the  $2 \times 1$  islands. Similarly, when Ag(110) is exposed to oxygen, one-dimensional linear Ag-O-Ag chains were observed (D71).

Niehus et al. studied the nitrogen-induced  $2 \times 3$  reconstruction of Cu(110) and discussed how the highly directional interactions between the Cu-N-Cu bonds determines the nature of the reconstruction (D72). Potassium-induced reconstruction of Cu(110) proceeds via homogeneous nucleation at low coverages and anisotropic growth along (110) at higher

coverages (D73). Ogletree et al. studied the sulfur-induced reconstruction of the basal plane of Re (D74, D75).

Roberts et al. found that air or water vapor injected into a controlled environment STM induced changes in the surface mobility of an annealed Au surface (D76). Hais et al. have imaged both the unreconstructed and  $\sqrt{3} \times 22$  reconstructed Au(111) surface in air and in triethylene glycol or propylene glycol (D77).

Gimzewski et al. studied the formation of antiphase boundaries on Au(110)  $1 \times 2$  and found that the nucleation and growth of the  $1 \times 2$  phase occurs predominately by mass transport via kink sites (D78). These authors also discuss the importance of domain boundaries in stabilizing unfavorable surface structures (D79). The influence of steps on the formation of missing-row reconstructions of Au(991) has been reported (D80). Au(991), which is a vicinal Au(110) surface with (111) steps parallel to the close-packed rows, has terraces which can accommodate two missing rows. In addition, extended regions of the stable Au(551)  $1 \times 2$  phase were observed.

**Miscellaneous Studies.** Ion implantation of noble gases in metal surfaces frequently generates surface defects that can be readily identified by STM. Michely and Comsa observed, for instance, that bombardment of Pt(111) with 1-keV He<sup>+</sup> ions caused vacancy islands, an increase in the density of dislocations, a large density of hexagonal adatom islands, and raised surface areas with subatomic heights resulting from He bubble formation (D81). Kr<sup>+</sup> implanted into Ti also produced a raised surface in areas where ions had implanted (D82). Michely and Comsa also examined the morphology of Pt(111) surfaces as a function of annealing time both before and after sputtering with 600-eV Ar<sup>+</sup> ions (D83). A transition from pit formation to layer-by-layer removal of the Pt surface was observed, and the role of vacancies and thermally excited adatoms was discussed. Lang et al. studied the erosion of Au films bombarded with Ne<sup>+</sup> and derived energy-dependent sputter yields and crater size distributions from STM images (D84).

Tench et al. compared clusters formed in laser-induced ablation of Si, SiC, Pt, and UO<sub>2</sub> and evaporation of UO<sub>2</sub> using laser ionization time-of-flight mass spectrometry and STM. All the clusters observed in the STM images were approximately the same size, making STM a questionable technique for identification (D85). Scandella et al. studied the Ar<sup>+</sup> ion etching and aplat-cooling of Nb<sub>50</sub>Ni<sub>50</sub> alloy nanocrystallites and the effects of laser quenching on the crystal morphology (D86). The use of ballistic electron emission microscopy has been reported in investigations of metal-metal and metal-semiconductor interfaces (D87-D89).

Ohmori et al. observed that Pd underwent morphological changes in the presence of electrochemically adsorbed hydrogen, including the development of the  $\beta$ -phase and nodular-like structures (D90). Besenbacher et al. characterized the morphology of an Fe-based NH<sub>3</sub> synthesis catalyst (D91). DeKoven and Meyers found that polycrystalline Fe surfaces exposed to perfluorodimethyl ether exhibited two distinct friction coefficients which corresponded to two morphologically different regions on the surface (D92). Endo et al. have obtained atomic resolution images of Pd, Au, and Mo under diffusion pump oil after etching in HF and conclude that the oil maintains a clean, flat metal surface (D93). Rice and Moreland used STM to image the magnetic ferrofluid particles on the surface of a hard disk (D94). Tang et al. have investigated terrace structures on Pt/Co multilayer thin films deposited on glass by Ar and Xe sputtering (D95). The features observed by STM are interpreted in terms of the energy distribution of the inert gas atoms.

Screw dislocations, Lomer-Cottrell locks, stacking fault tetrahedron, etc. on Ag(111) have been investigated by STM (D96). Everson et al. have studied the differences in the local density of states (DOS) on flat Au(111) as compared to that on monoatomic steps and pits and narrow terraces in UHV (D97). Monoatomic steps show a decrease in the surface DOS while narrow terraces have essentially the same surface DOS as the flat Au(111) plane. Fractal growth of Au deposits has been investigated using STM (D98).

Lankford and Longmire characterized the fatigue fracture surface of a stainless steel with the microfractures in a SiC fiber-reinforced Ti,Al composite and compared the results with those obtained from SEM images (D99). Komarica and

Kopp applied STM to the study of several stainless steels (D100).

The effect of surface plasmons on the tunneling current between a W tip and polycrystalline Ag film have been reported (D101). Plasmons results in an increase in the tunneling current of 50 pA and have a different dependence on the tunnel gap separation than the normal tunneling currents. Spectroscopic measurement of light emitted between various metallic tips and substrates was obtained by Smolyaninov et al. (D102). They found that the energy of emitted photons was less than the voltage applied to the tunnel junction and compared the voltage of the emission maximum to the surface plasmon energies in the junction. The angular dependence of the light emission intensity was monitored to investigate surface plasmon polaritons on an Au thin film (D103).

**D.2. Semiconductors.** Investigations of semiconductors by STM frequently includes correlation of surface features with the density of electronic states. The latter are measured by local tunneling spectroscopy (TS) or scanning tunneling spectroscopy (STS). Data are frequently presented as  $(dI/dV)/(I/V)$  vs  $V$  spectra, where  $I$  is the tunneling current obtained at a tip-sample bias,  $V$ . The quantity  $(dI/dV)/(I/V)$  represents the differential conductance  $(dI/dV)$  normalized to the integral conductance  $(I/V)$ . This method of plotting the  $I$ - $V$  data yield "spectra" that are correlated with electronic surface density of states (DOS). Fan and Bard, for instance, have obtained STM images and  $I$ - $V$  curves of a highly doped n-type FeS<sub>2</sub> (001) crystal in air (D104). The  $I$  vs  $V$  data are discussed in terms of the band locations, localized states in the band gap, and band bending. In other studies, STM is used in conjunction with photon biasing to obtain electronic parameters and to measure minority-carrier losses at surface defects (D105). Zhao et al. have used STM, STS, and optical spectroscopy to characterize CdSe particulate semiconductor films on dioctadecyldimethylammonium bromide monolayers (D106). In these studies, STM was used to determine the size of the CdSe particles and their degree of interconnectivity, while the spectroscopic data were employed to quantify the rectifying semiconductor behavior of the ensemble. In similar studies, the morphology and spectroscopic properties of size-quantized CdS and ZnS particles on various substrates including cadmium arachidate, zinc arachidate, or metal-ion-coated monolayers was investigated (D107, D108).

Feenstra and Lutz have used STM to study the transformation of the Si(111)  $2 \times 1$  structure to the  $7 \times 7$  structure as a function of time and annealing temperature (D109). An observed  $5 \times 5$  structure is consistent with the dimer-adatom-stacking-fault model; a  $\pi$ -bonded chain structure is confirmed for the  $2 \times 1$  structure (D110). Theory predicts that buckling in the  $\sqrt{3} \times \sqrt{3}$  reconstruction lowers the surface energy of the Si(111) surface; however, the lower energy  $2 \times 1$   $\pi$ -bonded chain reconstruction can occur if defects are absent (D111). First-principle electronic states calculations have been used to simulate the negative differential resistance observed in STS data on the Si(111)  $\sqrt{3} \times \sqrt{3}$  structure (D112). Kitamura et al. have observed the  $1 \times 1$  to  $7 \times 7$  surface reconstruction of Si thin films above 800 °C and report step formation and migration during the process (D113). Tarrach et al. have studied the Si(111)  $7 \times 7$  and Si(001)  $2 \times 1$  reconstructions in the vicinity of step edges and have observed buckled dimers on the latter surface (D114). In addition, they have investigated the structural transitions on laser-irradiated Si(111). Knall et al. have imaged the empty and filled states in the Si(113) surface and conclude there is strong evidence for a  $3 \times 2$  unit cell and explain reports of a  $3 \times 1$  reconstruction in terms of the density of domain boundaries (D115). Sugihara et al. have observed individual dimer atoms, in the occupied state images of Si(100) and discuss the role of elastic deformations on the observed image (D116). A Ginzburg-Landau model is used to model discrepancies between STM images, theory, and scattering experiments. In this latter study, the Si dimers are allowed to assume a tilted configuration (D117). Brocks et al. have also used first-principle total-energy calculations to calculate the activation energy for diffusion of an Si atom parallel (0.6 eV) and perpendicular (1.0 eV) to the dimer rows on Si(100) and propose that one-dimensional hopping of adatoms should be observable at low temperatures using STM (D118).

STM and STS data have been reported for oxidized n- and p-type Si(100) and p-n junctions formed by implantation of

P into B-doped Si wafers (D119). Kordic et al. have used a two-dimensional STM to image the contrast between p- and n-type regions in a biased Si p-n junction (D120). Hessel et al. have mapped the distribution of dopant around an implantation mask edge and found high doping levels corresponded to an ohmic *I-V* curve, whereas, low doping levels displayed a Schottky barrier behavior (D121). STM has also been used to measure the three-dimensional impurity profile of B in a metal-oxide-silicon structure (D122). Comparison of this method to results from secondary ion mass spectrometry and spreading resistance methods shows that the activated boron impurity concentration is measured rather than the total boron concentration.

Several authors have used STM to measure the surface photovoltages of semiconductors such as Si(111), Si(100), InP(100), and GaAs(100) when illuminated with laser irradiation (D123, D124) or monochromatic light (D125).

The mechanism of adsorption and desorption of H and O on Si is of interest in microelectronics processing (D126-D132). STM images suggest a SiH<sub>3</sub> species on the Si(111) surface after exposure to HF (D133). AFM images of Si etched in 48% HF show a disordered surface, while those etched at pH 5.5 or 9 in HF/NH<sub>4</sub>F show a well-ordered hexagonal structure (D134, D135). In addition, differences exist in the surface morphology of etched Si surfaces after exposure to aqueous solutions of differing pH's. Carrejo et al. studied the fractal topography of polysilicon films under dilute HF solutions and observed that the surface roughness increases with film thickness (D136).

Avouris and Lyo have studied the interaction of Si(111) 7 × 7 with H<sub>2</sub>O and O<sub>2</sub> and propose a dominant dissociative chemisorption mechanism for the H<sub>2</sub>O interaction (D137, D138). Pelz and Koch have proposed a two-stage mechanism for O reacted on Si(111) 7 × 7 at 300 K, based on topographic images (D139). Annealing the surface at 625 K changes the number and site preference of the two stages markedly. Kobayashi and Sugii proposed that the thermal desorption of native oxides on Si(111) occurs by the formation and lateral growth of voids rather than layer-by-layer growth, in agreement with RHEED and AES measurements (D140). TS data on ultrathin SiO<sub>2</sub>/Si structures and H-terminated Si surfaces yielded normal and defect site spectra in the former case but only normal spectra in the later case (D141). The defect spectra show negative differential resistance, which has been ascribed to resonant tunneling through localized defects in the oxide.

Several researchers have used STM to study the topography and electronic properties of faults (D142), kinks (D143), grain boundaries (D144), and steps (D145-D150) as well as step motion (D151, D152) on Si and compared these properties to theoretical calculations (D153-D156). Hartmann et al. have discussed the usefulness of the STM as a tool to study the roughness and surface topography of polished Si wafers (D157).

Nucleation and growth of Ge overlayers is described for Si(111) 7 × 7 (D158) and Si(001) (D159) substrates. Mo and Lagally investigated the anisotropy in the surface migration of Si and Ge on Si(001) and found that surface migration is >1000 times faster along the substrate dimer rows than perpendicular to them (D160, D161). Alvarez et al. have studied the inhomogeneous growth of FeSi and FeSi<sub>2</sub> grown on Si(100) using STM and find that the presence of surface steps on the Si induces a more epitaxial growth (D162).

Klitner et al. studied the oxidation of Ge(111)-c 2 × 8 as a function of temperature and found that at room temperature the primary nucleation sites are boundaries between domains of different orientations of the c 2 × 8 reconstruction, defects, and disordered adatom regions (D163). At higher temperatures, the oxide nucleates uniformly suggesting that the c 2 × 8 reconstruction is degraded at elevated temperatures. Hirschorn et al. observed buckling of the Ge(111)-c 2 × 8 surface upon annealing (D164). Conversion of the Ge(111) 2 × 1 surface into the c 2 × 8 surface upon annealing has been reported (D165). Surface disorder in the c 2 × 8 region, was suggested to be the result of surface adatom diffusion in the (001) direction (D166).

Heteroepitaxial films of Ge on Si(100) (D167), GaAs on InP(001) (D168), InGaAs on GaAs(100) (D169, D170), GaAs on GaP(001) (D171), Sb on GaAs(110) and InP(110) (D172), Bi on GaP(110) (D173), and As on Si(100) (D174) have also

been investigated by electron-tunneling techniques

Multiquantum well (MQW) structures, such as GaInAs InP (D175-D177), GaAs/AlGaAs (D178, D179), and InGaAs InAlAs (D180) and the effect of doping these structures have been investigated by STM. Electron-tunneling images of the MQW structures reflect the shape of the MQW potential.

Luminescence induced by electron tunneling has been used to study III-V heterostructures, such as Al<sub>1-x</sub>Ga<sub>x</sub>As (D181-D183). Information on the band-bending, the conduction-band discontinuity at the interface, trapping centers associated with defects and impurities, etc. can be obtained using this technique.

Combined STM-luminescence studies which examine the surface morphology, including reconstructions, terrace widths, kinks, and steps, of GaAs(001) grown by MBE have been reported by a number of researchers (D184-D187). McCoy and Makaym have also performed Monte-Carlo simulations to model the MBE growth of the 2 × 4 reconstructed GaAs-(001) surface and find the results correlate well with STM images (D188). Similar STM studies are reported for GaAs(110) (D189, D190).

Bonnell et al. have used tunneling spectroscopy to detect the photoexcitation of charge carriers in wide band-gap semiconductors such as ZnO and cubic SiC (D191). Valence-to-conduction band transitions were detected for the SiC samples, while charge-transfer transitions from the dopant levels were observed for ZnO. In addition, the tunneling spectrum of ZnO was altered by continuous exposure to ultraviolet light. Rohrer et al. also have used spatially resolved TS to investigate the effect of different surface treatments (e.g., annealing and exposure to air) on terraces and grain boundaries of ZnO (D192). STM was used to investigate the geometric and electronic structure of ZnO(0001) (D193). Steps on the surface, which are composed mainly of (1010) and (1120) faces, introduce mid-gap electronic states in the *I-V* curves.

The atomic arrangement and defects on n- and p-PbSe(100) as well as MBE layers of PbSe on BaF<sub>2</sub> have been investigated by STM (D194). In the case of the MBE layers, the (100) and (111) orientations of PbSe occur preferentially at specific substrate temperatures. Foecke et al. have measured the crack-tip morphology and upsets along the flanks of the cracks in PbS and Si. They discussed the effect of STM tip geometry and scan conditions on the image of the resulting cleavage crack (D196).

Rohrer and Bonnell studied TiO<sub>2</sub> and monitored local variations in the surface Ti:O stoichiometry using STM (D196).

**D.3. Superconductors.** The microscopic properties and conductance spectra of single-crystal films of NbN have been studied at 4.2 K using STM (D197). By cooling the films under a magnetic field of 0.1 T, a vortex corelike structure was observed (D198). Low-temperature tunneling spectroscopy data on the Nb/InAs/Nb superconducting system shows how the local density of electronic states of the InAs layer was modulated by the superconducting Nb layer (D199). Thomsson et al. have used STM to monitor film smoothness and measure the thickness of NbCN tunnel junctions (D200). Chen et al. obtained images and spectroscopic data from 4 K to 400 K on Pb films and found that there are sharp changes from the expected N-I-S tunneling characteristics to normal tunneling conditions at certain regions in the film (D201). Using spectroscopic measurements obtained at low temperature, the density of electronic states in a superconducting vortex core in Nb<sub>1-x</sub>Ta<sub>x</sub>Se<sub>2</sub> has been measured as a function of the disorder in the system (D202).

Several researchers have used AFM and STM to investigate the growth, surface structure, including the presence of dislocations and their effect on flux pinning, and effect of etching of YBa<sub>2</sub>Cu<sub>3</sub>O<sub>7-δ</sub> films and superlattices of YBa<sub>2</sub>Cu<sub>3</sub>O<sub>7-δ</sub> and PrBa<sub>2</sub>Cu<sub>3</sub>O<sub>7-δ</sub> (D203-D208). Moreland and Rice have used low-temperature tunneling stabilized magnetic force microscopy, where the tunneling tip is made of a flexible magnetic material, to image the topography and magnetic forces on samples of YBa<sub>2</sub>Cu<sub>3</sub>O<sub>7-δ</sub> (D209). Preliminary data show that large magnetic forces are acting on the tip during scanning at 48 K. STM and AFM have also been used by several researchers to characterize the morphology, tunneling characteristics, effect of O depletion, and effect of etching at room and low temperatures of Bi<sub>2</sub>Sr<sub>2</sub>CaCu<sub>2</sub>O<sub>8</sub> superconductors (D210-D217). Samanta et al. have imaged the incorporation

of O into a high- $T_c$  Bi/cuprate-based superconductor and use TS data to relate this phenomenon to the subsequent decrease in the  $T_c$  of the superconductor (D218). Wang et al. have characterized the morphology of superconducting Pb-Bi-Sr-Ca-Cu-O single crystals using STM (D219). Surface etching of single-crystal  $Tl_2Ca_2Ba_2CuO_8$  in air has been observed using STM (D220). STM has also been used to identify the metallic near-trigonal and semiconducting orthorhombic structures of  $Tl_2Ca_2Ba_2Cu_3O_{10}$  and  $Tl_2Ca_2Ba_2Cu_3O_{10}$  single crystals (D221).

**D.4. Layered Compounds.** Layered metals and semiconductors can be cleaved to yield large-area, atomically flat surface regions that are ideal for high-resolution AFM and STM studies. In addition, the materials and electronic properties of layered compounds, accentuated by their low dimensionality, is rich but less well investigated than most conventional metals and semiconductors. In particular, charge density waves (CDW) and other supramolecular surface structures resulting from crystallographic mismatch of the outermost surface layers has been heavily researched during the past years.

Parkinson et al. have imaged the periodic distortion caused by the van der Waals interaction between epilayers of transition-metal dichalcogenides (TMD's) grown by molecular beam epitaxy onto other TMD's (D222). Epilayers of  $MoSe_2$  deposited on various substrates by van der Waals epitaxy show novel surface structures which result from lattice mismatch (D223). Heckl et al. used STM, AFM, and SIMS to investigate 2-nm scale ring structures on the surface of naturally occurring  $MoS_2$  (D224). The differences between the natural and synthetic (ringless) forms of the material are discussed in terms of the fossilization process and electronic effects caused by point defects.

The observation of a negative differential resistance in the current-voltage curves for  $2Hb-MoS_2$  in UHV has been discussed in terms of a perturbation of the energy density of states by a contamination-induced peak, charging of electron traps, and resonant tunneling in a double-barrier quantum well structure (D225). Parkinson et al. have discussed atomic resolution STM and AFM images of  $ReSe_2$  in terms of DOS calculations and proposed four crystallographically distinct surface Se atoms (D226).

Wu and Lieber have used variable-temperature STM to investigate the nearly commensurate charge density wave (CDW) phase in  $1T-TaS_2$ . The commensurate CDW has a hexagonal domain structure whose period was temperature dependent (D227). Slough et al. found that the CDW amplitude in  $1T-TaS_2$  at room temperature shows a long-range modulation which gives rise to a two-dimensional pattern of domainlike regions rotated with respect to the CDW superlattice (D228). Burk has also imaged the domain structure in the nearly commensurate CDW phase of  $1T-TaS_2$ . The fine satellite structure has been identified using Fourier-transformed STM images, in agreement with the amplitude-domain and phase-domain model of Nakaniishi and Shiba (D229). Nb impurities in the incommensurate CDW phase in  $1T-TaS_2$  have been shown to cause dislocations resulting in random rotations of the CDW. The results are discussed in terms of weak pinning and the existence of a hexatic CDW phase (D230). Sakamaki et al. have observed the structure of a stacking boundary of nearly commensurate CDW's in  $1T-TaS_2$  caused by intercalated Ta atoms (D231).

Garnes et al. have used AFM to image the commensurate CDW structure on  $1T-TaSe_2$ , the incommensurate CDW structure on  $1T-TaS_2$  and  $1T-TiSe_2$ , and  $2H-NbSe_2$  (the latter does not show a CDW) at room temperature (D232). Three types of CDW vertices (triangular, rhombic, and hexagonal) imaged on  $1T-TaSe_2$  in air at room temperature have been described (D233). Using atomically resolved STM images, Gammie et al. have analyzed the structure of  $o-TaS_2$  (D233a). Dai et al. have shown that the three pairs of chains in the  $NbSe_2$  unit cell all carry a strong CDW modulation at 4.2 K, in disagreement with previous results (D234). At higher temperatures, the CDW is localized on only one pair of chains. Synchrotron single-crystal intensity data suggest a difference in the CDW modulation along the different chains in  $NbSe_2$  (D235, D236). Wang et al. have measured the CDW energy gap in  $1T-TaSe_2$ ,  $1T-TaS_2$ ,  $1T-VSe_2$ ,  $1T-TiS_2$ ,  $2H-TaSe_2$ ,  $2H-TaS_2$ , and  $2H-NbSe_2$ , and find a systematic dependence of the CDW strength on the materials properties (D237).

Akari et al. have monitored the growth and orientation of equilateral triangles from clusters following a voltage pulse applied between the tip and an atomically flat  $WSe_2$  surface (D238). All the triangles were found to have the same orientation with respect to given orientation of the substrate, reducing the 6-fold symmetry at the atomic Se surface to that of 3-fold symmetry at the molecular  $WSe_2$  layer. Van Bakel et al. have imaged the trigonal symmetry of the  $TiS_2$  lattice as well as several other new features (D239). A model involving displacement of Ti atoms is presented to account for the observed features.

Saulys formed pits in the surface of  $Na_0.9Mo_6O_{16}$  by briefly increasing the bias voltage or tunneling current between the tip and the sample (D240). Explanations for the change in the pits with time, forming either faceted or rounded shapes, are discussed. Rudd et al. have also imaged  $Na_0.9Mo_6O_{16}$  and  $Rb_0.9MoO_3$  and discuss their images in terms of the defect creation techniques, the relative defect stabilities, and CDW's of these materials (D241).

**D.5. Carbon.** Because of the ease of surface preparation, highly oriented pyrolytic graphite (HOPG) continues to be frequently used as a substrate for imaging molecular adsorbates. Clemmer et al. (D242) and Chang et al. (D243), however, have imaged a number of anomalous surface features on bare graphite surfaces which are strikingly similar to structures previously identified as molecular adsorbates, including images of DNA and polymers published in the late 1980's. These researchers discussed general problems associated with using HOPG as a substrate.

Siperko used STM to observe various features, including hexagonal etch pits, steps, and crystals, on graphite surfaces including HOPG, pyrolytic graphite, benzene-derived graphite, and triphenylene-derived graphite (D244). Several authors have imaged superperiodic hexagonal domains on the surface of HOPG both in water and under solution (D245-D248). Myrick et al. showed that TS data taken from defect areas on graphite have a lower surface density of states and suggest that TS data may make the distinction between defects and molecular adsorbates easier (D249).

Brown and You have used STM to characterize the morphology of glassy-carbon surfaces. Two types of structures exist in addition to the normal graphite structure, one being a granular structure with grain sizes from 80 to 250 Å and the other consisting of a curved fibrillar structure (D250).

Olk et al. have imaged a stage-1 graphite intercalation compound ( $C_8CuCl_2$ ) at both positive- and negative-sample biases with respect to the tip. At positive-sample biases, a hexagonal symmetry was observed (due to the ABAB stacking arrangement) rather than the 3-fold symmetry of nonintercalated HOPG. At negative-sample biases, a different image was obtained where the pattern is mainly due to the intercalate layer and perturbed graphite (D251). A new orthorhombic superlattice was observed in stage-1  $KHgC_4$  compound. Kelty and Lieber have imaged and discussed the origin of a new commensurate  $2 \times 2$  superlattice in addition to the hexagonal graphite lattice in stage-1  $KHgC_4$  and stage-2  $KH_2C_8$  graphite intercalation compounds (D252). They have also imaged a commensurate  $2 \times 2$  and an incommensurate superstructure on  $KHgC_4$  and a one-dimensional superstructure and two-dimensional superlattice on  $KH_2C_8$  (D253).

The atomic packing, defect structures, and electronic structure of C epitaxially precipitated on Ni(111) was found to be essentially identical to that of HOPG (D254). Itoh et al. have used LEED and STM to study a monolayer of graphite epitaxially grown on TiC(111) and discuss TS data on the surface band structure of the monolayer (D255). Murata et al. have imaged a disordered carbonaceous film composed of benzene rings prepared by pyrolysis of cyclododecane on a quartz substrate (D256). Ito et al. found that carbon films synthesized by direct ion-beam deposition at 100 eV have the smoothest surface (D257). Vandentop et al. studied the nucleation and growth of hydrogenated amorphous carbon films on HOPG and silicon and observed a more homogenous growth on silicon (D258).

Numerous researchers have used STM or AFM to characterize the nucleation, growth, effect of doping, morphology, and  $I-V$  characteristics of chemically vapor-deposited diamond films (D259-D267).

The effects ion-bombardment of graphite surfaces was studied extensively during the past year as a function of the

ion flux and sample temperature (D268-D272). Surface modification of graphite surfaces in air and in liquids has been reported by several authors (D273, D274). STM has been used to correlate the morphology of carbon electrodes after laser-activation with measured electrochemical heterogeneous charge-transfer rates (D275-D277). These activated surfaces exhibited a significant increase in the surface roughness and number of defect sites. Carbon electrodes can also be electrochemically activated by application of an applied voltage (D278). STM and AFM images of the activated surface showed an increase in the surface roughness suggesting the presence of an oxide layer.

Chang and Bard have investigated the oxidation of the graphite surface at elevated temperatures and monitored the nucleation and growth of etch pits. In addition, they also concluded that the formation of etch channels on the graphite surface after treatment using both chemically active (e.g. FeCl<sub>3</sub>, CdS, and H<sub>2</sub>PtCl<sub>6</sub>) and inactive (e.g., NaCl and Al<sub>2</sub>O<sub>3</sub>) compounds were primarily the result of mechanical interactions of the particles with the graphite surface (D279).

Hoffman et al. have investigated the roughness and structure of several C fibers, including type-II polyacrylonitrile (PAN)-based fibers and type-II pitch-based fibers, and the effect of heat treatment on these fibers (D280). Hoffman et al. have also investigated the effect of various treatments, including O exposure at high temperatures, O and Ar plasma exposure, HNO<sub>3</sub> exposure, and electrochemical treatment on the morphology of P-55 pitch-based C fibers (D281).

**D.6. Atomic and Molecular Adsorbates.** Eigler et al. used low-temperature STM to image individual Xe atoms on Ni(110) and found the apparent height of the Xe atom in the STM image was in agreement with the expected value based on an atom-on-jellium model (D282). They also note that the Xe 6s resonance, which is the origin of the Fermi-level local density of states, is responsible for the observed contrast in the STM image. Eigler et al. have developed a prototype of an atomic bistable switch based on a Xe atom which, by applying a voltage pulse of a particular sign, can be positioned on either the STM tip or Ni surface (D283). This prototype system has potential applications for manufacturing small electronic devices. (see "Surface Modifications", below). Whitman et al. have demonstrated the manipulation of adsorbed Cs atoms on GaAs and InSb by application of a voltage pulse between the tip and sample (D284).

Hallmark et al. investigated the molecular orientations and rotations of naphthalene on Pt(111) at room temperature in UHV (D285). Magonov et al. investigated the morphology of thin layers of 2,3-Fe-naphthalocyanine vapor deposited on amorphous carbon (D286). Regions of disorder as well as arrays of stacks with periodicity of 0.4 nm in a row and 1.5 nm between stacks were observed. Individual molecules of the ferromagnetic crystal, 2-(4-nitrophenyl)-4,4,5,5-tetramethyl-4,5-dihydro-1H-imidazolyl-1-oxo 3-oxide, were imaged with AFM and the molecular arrangement was found to be in agreement with the bulk crystal structure (D287). Nejh has studied the incremental charging of a single molecule of a liquid crystal at room temperature and observed quasi-periodic variations in the current-voltage curves which were attributed to a change in the charge of the molecule (D288).

STM has been used in conjunction with electron microprobe analysis, SIMS, and ATR to study the adsorption of CO on Pt and Pd (D289). Other studies concerning CO adsorption are discussed below in the section on "Electrochemical STM and AFM."

**D.7. Polymers with Quasi-Crystalline Films.** *Polymer Processing.* AFM has been used to monitor the processing defects, laser conditioning and aging, and laser beam damage in e-beam evaporation deposited antireflection and high-reflection coatings (E290). STM has been used to determine whether resolution degradation occurring in undeveloped e-beam resist (polydiacetylene negative resist) occurs during the exposure to the 50-kV e-beam or during resist development (E291).

AFM of polyethylene (I) rods during extrusion showed the surface parallel to the extrusion direction consisted of ziggzag chains (D292). Smaller scans showed the structure of individual microfibrils including defects in the chains. Individual methylene groups have also been resolved in these samples (D293). Noncontact force microscopy was used to investigate the aging of glassy polymers including polystyrene (I) and

poly(2,6-dimethylphenylene oxide) (D294). Zhai et al. have used AFM to monitor the radiation damage caused by heavy ions on the surface of a polycarbonate film (D295).

Lee et al. have used a variety of techniques including STM to show that implanting Kapton H, Teflon PFA, Tefzel, and Mylar with ions such as B, N, C, Si, and Fe improves their smoothness, hardness, and wear resistance (D296). Using a special imaging mode of the STM, based on charge trapping, the degree of uniformity of a perfluoropolyether film on magnetic thin-film rigid disks was examined and found to be nonuniform near scratched regions (D297).

Lotz et al. have used AFM to image the lamellar structure of  $\alpha$ -phase isotactic polypropylene epitaxially crystallized on benzoic acid (D298). Yang et al. have used STM to image helical and superhelical structures in poly(ethylene oxide) complexes containing KI and NaI (D299). Mate and Novotny have used AFM, XPS, and ellipsometry to show that physisorbed fluorocarbon polymers have an extended structure on solid surfaces (D300). The disjoining pressure of a monolayer of polymer was measured by AFM. Dietz et al. have used AFM to image polysulfone and polyether-polysulfone ultrafiltration membranes of different sizes in the dry state and in the presence of water (D301).

*Electroactive Polymers.* STM has been used to correlate the XPS depth resolution to the sputter-induced roughness in AgNO<sub>3</sub>-doped electrochemically prepared films of Fe-(vbpy)<sub>2</sub>(CN)<sub>2</sub> homopolymer-poly(vbpy) blends (vbpy = 4-vinyl-4'-methyl-2,2'-bipyridyl) (D302).

Madsen et al. have measured the increase in the surface area of electrochemically prepared polypyrrole films grown on a Pt electrode by several methods including ac impedance measurements, SANS, and STM (D303). The first two techniques indicate an increase in the surface area of 40-50 times relative to Pt while the STM measurements show only a 2.2-fold increase. Everson and Helms have shown that the electrochemical growth of thin films of perchlorate-doped polypyrrole on HOPG starts as small islands nucleating near defect sites (D304).

Porter et al. have imaged both chemically and electrochemically prepared borate-substituted polyanilines. They observed that the chemical preparation resulted in small amorphous conducting domains as well as nonconducting domains, while the electrochemical preparation yielded conducting amorphous islands and polymer coils (D305). Porter et al. have also imaged amorphous islands and polymer strands in samples of chemically and electrochemically prepared poly(3-hydroxyaniline) thin films (D306). Jeon et al. have studied the growth of thin films of electropolymerized polyaniline on evaporated Au electrodes and have measured the  $\pi-\pi^*$  gap of the fully protonated emeraldine salt form of polyaniline (D307).

Armes et al. have studied the morphology and coating homogeneity and discussed the mechanisms of conduction in polyaniline and polypyrrole colloids, polyaniline- and polypyrrole-coated textile substrates, and electrochemically synthesized polyaniline films using a combination of STM, TEM, SEM, and X-rays (D308). These researchers have used a variety of techniques to characterize several polypyrrole-quartz and polyaniline-quartz composites; STM shows that the polymer films are thin and uniformly deposited over the quartz (D309).

Kamrava et al. have imaged FeCl-doped polythiophene, I-doped Shirakawa polyacetylene, and thin films of undoped poly(4,4'-dibutyl-2,2'-bithiophene) (D310). The polythiophene has a lamella-like structure and shows low or undoped islands surrounded by highly-doped regions. Mizes et al. have used STM and AFM to image the growth and fibrillar nature of films of doped and undoped polyacetylene poly(3-hexylthiophene) and polystyrene and discussed the limitations of these techniques in obtaining atomic resolution (D311). Fuchs et al. imaged poly(1-butene)(I) films on HOPG and have observed 100-nm flakes (D312). Oka and Takahashi observed the slightly collapsed, global shape of iodine-doped poly(N-vinylcarbazole) deposited on HOPG; however, they were not able to resolve any details of the polymer structure (D313). Wang et al. studied the effect of different anodization conditions on the morphology and conductivity of polyphenol layers on GC surfaces (D314). Yang et al. have studied chain conformation, nucleation and film growth, and the effect of counterion doping on polypyrrole/poly(4-styrenesulfonate)

on graphite and Au/Si surfaces (D315).

**Molecular Films.** Several authors have used STM to investigate the ordering of liquid crystals, such as the alkylcyanobiphenyls, on various surfaces, including MoS<sub>2</sub> and graphite (D316–D321). Nejob has also investigated the orientation and chemical bonding of liquid crystals on a polyimide surface by several techniques including XRD, STM, and XPS and compared these results to self-consistent MO calculations (D322).

C<sub>60</sub> has been imaged on both Au and graphite substrates (D323). Chen et al. have obtained high intramolecular contrast in imaging a monolayer of C<sub>60</sub> on Au and find that every other C atom is imaged (D324). STM images of C<sub>60</sub> overlayers on GaAs(110) show a well-ordered structure, commensurate with the GaAs surface, and two types of adsorption sites, one being elevated due to stress in the C<sub>60</sub> monolayer (D325). Li et al. have used STM to study the differences in monolayer and multilayer structures of C<sub>60</sub> grown on GaAs(110) at various temperatures and the effect of potassium incorporation into C<sub>60</sub> (D326). Snyder et al. have used AFM to image C<sub>60</sub> deposited on CaF<sub>2</sub>(111) (D327).

Leung et al. have used STM to image both single chains and ordered monolayers of polydiacetylene, which has nonlinear optical properties, on HOPG and discuss the role of H bonding between polymer chains (D328). Hawley and Benicewicz have investigated the attachment of rigid pendent groups to the polymer backbone and the effect of salt concentrations on the morphology of a wholly aromatic polyamide deposited on HOPG (D329). Fujiwara et al. have imaged a polyimide LB film based on pyromellite dianhydride and 4,4'-oxydianiline on graphite and compared the alignment of the polymer chains to molecular dynamics calculations (D330).

Hanama et al. discussed the usefulness of the AFM in determining the thickness and quality of LB films and presented images of Cd arachidate monolayers on mica showing surface defects (D331). Bourdieu et al. have used AFM and optical microscopy to characterize LB films of arachidic acid and found that the film roughness and thickness of the bilayers corresponds to the fully extended aliphatic chains on the substrate (D332). Meyer et al. have also obtained AFM images of Cd arachidate (on Si) and suggest that the organized film has an orthorhombic or monoclinic crystal structure which is independent of the substrate periodicity (D333).

Weisenhorn et al. have imaged LB films of the lipids DL- $\alpha$ -dimyristoylphosphatidylethanolamine, L- $\alpha$ -dimyristoylphosphatidylglycerol, dioctadecyldimethylammonium bromide (DODAB), and 1:1 DODAB/L- $\alpha$ -dipalmitoylphosphatidylglycerol with molecular resolution under buffer solution using AFM (D334). The authors present images of DNA adsorbed on these films and discuss their usefulness as substrates for binding other macromolecules.

Yang et al. have obtained atomic resolution STM images of poly- $\alpha$ -D-glucose which show only oxygen atoms and discussed this result in terms of X-ray diffraction studies (D335). McMaster et al. have imaged an ordered crystalline array of poly( $\gamma$ -benzyl L-glutamate) and discuss the role of the benzyl substituents in the observed  $\alpha$ -helical structure (D336). Shigekawa et al. observed that inclusion molecules (1-adamantanemethanol) added to a mixture of  $\alpha$ - and  $\beta$ -cyclodextrins, which form an ordered array on HOPG, results in the disruption of the regular structure (D337). Heckl and Smith have applied a high electric field to a thin film of glutaraldehyde on HOPG to form clusters and suggested that this may cause the electropolymerization of the molecules (D338). They extend their results to a discussion of the role of lateral charge transfer in imaging low-conductivity samples.

Vandenberg et al. have used STM to study the morphology of (3-aminopropyl)triethoxysilane films deposited on SiO<sub>2</sub> surfaces under various conditions of solvent, heat, time, and curing environments (D339).

Dawson et al. have used STM to measure the surface roughness of benzoic acid derivatives on thermally evaporated Ag films as a function of deposition rate (D340). Rabe and Buchholz have imaged the lamellar structure of long-chain alkanes, alcohols, fatty acids, and dialkylbenzene on HOPG (D341). McGonigal et al. have also imaged the two-dimensional ordering of *n*-alkane and *n*-alkanol layers on HOPG (D342). Armstrong and Muller have used STM to investigate benzotriazole films on Cu (D343). LB films of behenic acid, a fatty acid bilayer, deposited on HOPG show two types of

periodic molecular arrangements (D344). Rabe and Buchholz have used STM to investigate the motion of domain boundaries within a molecular monolayer which forms a 2D polycrystal at the interface between the basal plane of graphite and a solution of didodecylbenzene (D345). AFM images of platelet-type monocrystals of linear alkanes, *n*-tritriacontane, *n*-hexatriacontane, cyclic alkanes, cyclooctatetracontane, and cyclododecaheptacontane all showed a regular surface structure (D346).

Widrig et al. have obtained atomic resolution of monolayer films of ethanethiol and *n*-octadecanethiol adsorbed on Au(111) (D347). These latter films form hexagonally packed arrays, in agreement with He diffraction data which shows a  $\sqrt{3} \times \sqrt{3}$ -R30° structure. Defect structures in a self-assembled insulating monolayer of CH<sub>3</sub>(CH<sub>2</sub>)<sub>11</sub>-SH on Au(111) have been imaged by electrochemically depositing metal islands in the defect areas (D348). DeKoven and Meyers found that polycrystalline Fe surfaces exposed to perfluorodiethyl ether exhibited two distinct friction coefficients which corresponded to two morphologically different regions on the surface (D349).

Keita and Nadjo have imaged a regular periodic pattern of H<sub>3</sub>PW<sub>12</sub>O<sub>40</sub> deposited on HOPG, suggesting that individual molecules are imaged (D350). Weinrach et al. discuss the superstructure and CDW superstructure observed in images of a trapped-valent linear-chain semiconductor K<sub>4</sub>[Pt<sub>2</sub>(P<sub>2</sub>O<sub>5</sub>H<sub>2</sub>)<sub>4</sub>Br]·3H<sub>2</sub>O (D351).

**Miscellaneous Studies.** Li and Lindsay have devised a lateral and vertical calibration standard for the AFM (for the nanometer to micron range) which involves the deposition of polystyrene latex spheres onto mica to form crystalline layers in a cubic or hexagonal close-packed arrangement (D352).

The morphology of a monolayer of Ag particles formed in situ in aqueous Na bis(ethylhexyl) sulfosuccinate and Ca alkylarenesulfonate surfactant reversed micelles and deposited onto a solid substrate was determined by STM and dynamic light scattering (D353).

STM and AFM have been used to characterize the morphology and thickness of illite/armectite particles from the North Sea Jurassic oil source rock (D354).

Rauf and Walls have compared TEM and STM images of ITO films and found that the two techniques give generally consistent data; however, the grain size in the STM images is larger than in the TEM images (D355).

**D.8. Crystalline Molecular Solids.** STM studies of several different conductive organic charge-transfer systems, including TCNQ complexes, polymeric complexes, organic superconductors, and the charge-transfer complexes of TCNQ-salts have been reported (D356–D362). The morphology and electronic properties of BEDT-TTF [bis-(ethylenedithio)tetrafulvalene] and TMTSF (tetramethyltetraselenafulvalene) charge-transfer complexes have been extensively studied using STM and TS (D363–D370).

Overney et al. have used AFM to assign lattice parameters and identify two translationally inequivalent molecules in the unit cell of a free-standing tetracene crystal (D371). Atomic resolution on different faces of the conductive perylene radical cation hexafluorophosphate crystals have also been obtained using AFM and STM and discussed in relation to crystallographic data (D372). AFM was used to examine the large-scale morphology and atomic structure of single-crystal poly[2,4-hexadiynylenebis(*p*-fluorobenzenesulfonate)] and its corresponding monomer (D373).

Gratz et al. have investigated the importance of ledge motion to the dissolution and growth of silicates and present AFM images during the dissolution of quartz (D374). Shindo et al. have used AFM to image the arrangement of O atoms and water molecules on the surface of cleaved gypsum (CaSO<sub>4</sub>·2H<sub>2</sub>O) (D375). AFM was used to image Kr ion tracks on mica. In this latter study, changes in the elastic properties of the mica could be deduced on a nanometer scale (D376).

Jensen et al. (D377) have used STM to image a zeolite pore in silicalite. MacDougall et al. (D378) have used AFM to image the crystal planes of several natural zeolites including scolecite, stilbite, and faujasite both in air and under aqueous solution.

Meyer et al. have obtained atomic resolution on surfaces of epitaxially grown AgBr(001) films using AFM and suggest that only Br atoms are imaged (D379, D380). AFM images of single-crystal sodium decatungstocerate(IV) indicates that only the (010) face of the crystal has a regular arrangement of anions (D381). AFM has been used to image the (001) and (100) faces of aspirin crystals in air and water to determine how the different molecular structures at each face relate to the differences in the dissolution rates (D382).

Slawska-Waniewska et al. have used STM to investigate the effect of ion irradiation on the morphology of FeCrSiB amorphous ribbons (D383). Fukumoto et al. have obtained atomic resolution STM images of hexagonal boron films grown on graphite by plasma chemical vapor deposition (D384).

**D.9. Biological Molecules.** Thompson and Elings have reviewed applications of STM and AFM in biological sciences (D385). Conductive organic monolayers and nucleic acids have been imaged on silicon (D386) using STM. Techniques to reduce tip-surface interactions, which can easily displace biomolecules and lead to irreproducible images, are discussed in the same report. Images of organic and biological molecules can be improved by immersing samples in a 50% glycerol-water solution (D387). Two-dimensional arrays of electroactive and photoactive proteins suitable for STM imaging have been prepared using either a Langmuir-Blodgett technique and/or adsorption method (D388). For example, using the Langmuir-Blodgett technique, densely packed quasi-regular mono and bimolecular films of gramicidin A were formed on HOPG. Single molecules were imaged which show a cavity of 0.4 nm in half-width, consistent with molecular models (D389).

Leatherbarrow et al. have used STM to examine immunoglobulin G (IgG) molecules deposited on graphite and confirmed their trilobed structure as shown in X-ray crystallographic images (D390). Unlabeled IgG antibodies complexed with Au-labeled antigen and Au-labeled IgG antibodies have also been imaged by STM. Details of their molecular organization have been reported (D391).

Images of glycogen, phosphorylase, and phosphorylase kinase on HOPG have been reported and correlated with measurements using other techniques; anomalously low values of the apparent height of these molecules are observed using STM (D392). STM has also been used to image phosphorylase kinase and dimers and oligomers of phosphorylase *b* immobilized on a charged HOPG surface (D393).

Miwa et al. investigated a  $\text{Ca}^{2+}$ -sensitive monolayer protein membrane prepared by conjugating calmodulin and bovine serum albumin at the air-water interface (D394). Depending on the  $\text{Ca}^{2+}$  concentration, the protein film changes from an extended structure (with  $\text{Ca}^{2+}$ ) to a contracted structure (no  $\text{Ca}^{2+}$ ) as a result of conformational changes in the calmodulin.

Images of tetrameric cytokeratin  $\alpha$ -helical protein (D395) and the globular proteins, lysozyme and chymotrypsinogen A (D396), deposited from solution on graphite have also been reported. In the case of lysozyme, a two-dimensional array is observed with a characteristic periodicity that is dependent on the initial concentration of the protein in solution. For chymotrypsinogen A, smaller areas consisting of a two-dimensional structure were also observed. Pizziconi and Page have imaged laminin, a 900 000 MW glycoprotein, in phosphate buffer on HOPG and confirm previous electron microscopy images showing the cruciform structure of the protein (D397). Yeung et al. imaged the lipoprotein ice nucleator (LPIN) from the hemolymph of *Tipula trivittata* and the non-ice-nucleating lipoprotein from *Manduca sexta* (D398). In the former case, the LPINs formed aligned chain structures with a width equal to two lipoproteins. Two apolipoproteins of the LPIN, Apo-I and Apo-II, were also imaged and have a platelike morphology. Amrein et al. have compared STM and TEM images of the hexagonally packed protein monolayer found in the outer cell wall of *Deinococcus radiodurans* (D399).

Zhu et al. imaged the right-handed helical structure of calf skin collagen molecules adsorbed on graphite and measured a periodicity of  $\sim 31$  Å, in agreement with previous biochemical studies (D400). Miles et al. imaged the spiral structure, based on  $\beta$ -reverse turns, of the elastomeric wheat gluten proteins (D401). Masai et al. observed the sheet-type paracrystal form of fibrous actin when deposited in the presence of  $\text{MgCl}_2$  on HOPG and allowed to air dry (D402).

One of the four DNA bases, guanine, was imaged in a two-dimensional ordered array composed of closed-packed linear chains of hydrogen-bonded molecules on HOPG and  $\text{MoS}_2$  substrates (D403). Images of aggregates, as well as individual molecules, of 16S rRNA electrophoretically deposited on HOPG in water were in agreement with EM data (D404). Keller et al. imaged RNA polymerase, from *Escherichia coli*, electrodeposited on atomically flat Au surfaces in both water-glycerol and high-humidity environments (D405). The molecule appeared as either ordered arrays, amorphous features, or jaw-shaped molecules. Time-dependent studies were done to determine the binding mechanism of the protein.

Imaging DNA under ambient conditions and in real time is one of the more popular research goals due to the potential for sequencing DNA using STM. Lindsay and Philipp have discussed the potential success and difficulties in using STM to sequence DNA (D406). (See also the section on "Carbon" regarding suspect molecular structures observed on HOPG.) DNA has been imaged in air on a graphite substrate during replication for the first time (D407). Youngquist et al. discuss contrast mechanisms for imaging DNA (D408).

Images showing atomically resolved features of the DNA molecule on HOPG are presented and compared to a model of the van der Waals surface. Uncoated DNA molecules with an activated tris(1-aziridinyl)phosphine oxide solution have been imaged on Au substrates. The molecules are several hundred angstroms long with a regular intraperiodicity of 25–35 Å (D409). High-resolution images show the phosphate groups on the DNA backbone in the minor groove. Cricenti et al. have reported tentative observations on the phosphate and sugar group components, as well as the bases, of uncoated single-strand DNA mixed with benzyldimethylalkylammonium chloride and deposited on Au substrates (D410).

A method for covalently attaching mercurated DNA to a -SH-modified graphite surface have been reported. The covalent attachment reduces the mobility of the DNA (D411). Bai et al. have identified several forms of DNA including a braided triple-stranded structure, right-handed and left-handed double helical forms, and a tertiary structure (D412). Li et al. have imaged the B-form of DNA from fish sperm and calf thymus and the poly(dG-m<sub>5</sub>dC) and bromized poly-dCG Z-form of DNA (D413). Allen et al. imaged synthetic DNA on HOPG following desorption of the DNA from the tunneling tip by a voltage pulse (D414). The DNA molecules appeared to be deposited singly or in highly oriented groups.

In tunneling spectroscopy experiments, Lindsay et al. adsorbed submonolayer quantities of DNA in tris(hydroxymethyl)aminomethane buffer onto Au electrodes and monitored the current vs voltage (*I*-*V*) curves over the DNA patches and the clean Au surface (D415). The *I*-*V* curves over the DNA patches did not depend strongly on the tip bias and display diodelike characteristics. Lindsay et al. have also deposited DNA onto graphite and Au modified with  $\text{Cl}^-$  ions and tris(hydroxymethyl)aminomethane buffer (D416). Reproducible results were obtained only for positively-charged Au modified electrodes in the presence of DNA fragments and the salt, making the images difficult to interpret.

AFM has also been used to study DNA as well as other biological molecules. Hansma et al. obtained AFM images of single-stranded DNA with nucleotide resolution using two different sample preparation techniques. In one method, the DNA was covalently attached to a polymerized lipid monolayer and subsequently imaged under water. The second method consisted of adsorbing DNA on mica, rinsing with a  $\text{Ba}(\text{NO}_3)_2$  solution, and imaging under ethanol (D417). The authors discussed problems associated with sequencing DNA using the AFM.

Friedbacher et al. obtained atomically resolved images of pressed powder samples of pismo clam and sea urchin shells using AFM (D418). Hanama et al. used AFM to obtain molecular resolution images of IgM and UV light-polymerized films of the lipid dimethylbis(pentacosadiynoyloxyethyl)ammonium bromide (D419). The polar head groups of the lipid could be imaged. Schmitt et al. used fluorescence microscopy and AFM to investigate the specific recognition and binding of a biotinylated lipid layer and streptavidin (D420). AFM and fluorescence microscopy confirm that streptavidin is adsorbed only to the fluid matrix of the compressed lipid monolayer at the electrolyte-lipid interface. The hydrated

protein surface layer of *D. radiodurans* has been imaged using the attractive imaging mode of the AFM (D421). Two forms of fibrinogen, a trinodular and globular form, have been imaged on SiO<sub>2</sub> surfaces using AFM (D422).

The photon scanning tunneling microscope (PSTM), which relies on the tunneling of photons from an evanescent wave to a sharpened optical fiber probe tip, is useful for examining electrically insulating samples including biological molecules. Ferrell et al. have constructed several PSTM's and presented preliminary images of *E. coli* (D423).

### E. SURFACE MODIFICATIONS

STM and AFM, which are based on physical interactions between the probe tip and the substrate, can alter and/or damage the surface being imaged. In favorable circumstances, tip interactions can be employed to intentionally modify the surface or to arrange molecular or atomic species in a specified pattern that introduces some desired interfacial property. Most research in this area during the past year focused on key issues underlying the mechanism of tip-induced surface alterations or on "proof of concept" demonstrations of manipulating nanometer-sized structures. Related articles are discussed in above sections on "Theory" and "Instrumentation and Probe Tips".

Alterations of metal surfaces during STM scanning has been reported by several groups. Ohmori et al., for instance, studied the morphological changes on samples of Pd and Pt and found that the surface roughness of these metals decreased during imaging (E1). The authors propose that electrostatic forces between the STM tip and metal surface are responsible for this phenomenon. Roberts et al. generated rectangular pits in polycrystalline Au by scanning a small portion of the surface at a high tip bias in an Ar atmosphere (E2). They also investigated the annealing of the pits as a function of time. The decay of surface plasmon polaritons in an Al-I-Au thin film tunnel junction, as evidenced by the decay of visible light emitted from the Au-air interface, was shown to result from smoothing by surface diffusion in areas where the tip contacted the surface (E3). Shear and compressive forces exist between the tunneling tip and sample surface during scanning and have been discussed in relation to anomalous corrugations and elastic and plastic deformations that are observed in STM topographic images, and in relation to anomalously low values obtained for tunneling barrier heights (E4). Meepagala et al. simultaneously measured the tunnel current and force between an Au-coated AFM tip and Au sample under atmospheric conditions and discuss the effects of surface contaminants (E5).

STM tips can also be used as miniature evaporation sources for atom deposition. Mamin et al., for example, have used a gold STM tip as a solid-state emission source for deposition of nanometer-sized Au clusters (E6). Field-ion STM (FI-STM) has been used to investigate the degree of adsorption of alkali metals (e.g., Cs, K, and Li) on Si(111) and Si(100) surfaces (E7, E8).

Surface modification at the nanometer scale has potential applications in the manufacture of information storage devices, although it is noted that current STM and AFM systems are too slow for any form of large-scale device manufacturing. Hartmann et al. have written electronically active nanometer-scale structures in a Si p-n junction using high current densities from an STM tip with the p-n junction biased in the forward direction (E9). Lithography on III-V semiconductor substrates using an STM probe has been discussed as a means of generating nanometer-scale oxide masks for use in the manufacture of low-dimensional heterostructures (E10, E11). Dobias and Marrian have compared the minimum developed line widths achievable by nanolithography with the STM tip (27 nm) with those obtained by exposure to a 17-nm 50-kV electron beam (95 nm) (E12). Using a STM, Casillas et al. have fabricated 5-36-nm-radius inlaid Pt disks on the surface of TiO<sub>2</sub> (E13) and Fuchs and Schimmel have demonstrated surface modification of atomically flat areas of a p-doped layered semiconductor, WSe<sub>2</sub> (E14). Nanometer-scale structures on graphite have been generated in the presence of Me<sub>3</sub>Al under different tip biasing and tunneling current conditions (E15).

Eigler et al. have demonstrated a prototype of an atomic bistable switch based on a Xe atom, which can be positioned on either the STM tip or Ni surface by applying a voltage

pulse (E16). Lyo and Avouris have also discussed the use of STM to fabricate new electronic devices by applying voltage pulses to the STM tip to manipulate atoms (E17).

### F. ELECTROCHEMICAL STM AND AFM STUDIES AND SCANNING ELECTROCHEMICAL MICROSCOPY

STM and AFM are particularly well-suited for studies of electrodes immersed in solutions, providing the first opportunities for electrochemists to examine, in situ, potential-dependent reconstructions and adsorption phenomena at the atomic and molecular level. Imaging systems for in situ studies were developed in the late 1980s and are not reviewed here: home-built and commercial STM's with capabilities for in situ electrochemical measurements generally allow for simultaneous control of the tip-to-substrate bias and the bias between the substrate and an electrochemical reference electrode. In addition, the tip in an electrochemical STM experiment must be insulated except at the very end in order to reduce background faradaic currents that interfere with measurement of the tunneling current. These difficulties are circumvented by use of AFM, which has been more frequently employed during the past few years.

Yaniv and McCormick reported an electrochemical system with potentiostatic/galvanostatic control of the sample and potentiostatic capabilities of the STM tip, and used this system to deposit Cu and Cd on HOPG and GC (F1). Application of the electrochemical STM in studies of the electrochemical double layer structure (F2) and use of imaging tunneling spectroscopy as a tool for spatial mapping of the surface electronic properties of electrodes in solution (F3) have been discussed.

Honbo and Itaya have studied, in situ, the electrochemical oxidation of Au(100) in aqueous perchloric acid and monitored the island growth mechanism of the AuOH layer (F4). Binggeli et al. have compared the morphology of electrochemically polished Au(111) electrodes in the presence and absence of Pb adsorbates during polarization of the electrode. The transition from tunneling to point contact was observed at a tunneling resistance of  $\sim 2 \times 10^4 \Omega$ , in agreement with vacuum results (F5).

Trevor and Chidsey studied at the annealing of Au(111) surfaces in an electrochemical cell using STM and found that the process was dominated by the motion of step-edge adatoms rather than terrace atoms. They suggest that pit motion results from random diffusion of step adatoms (F6). Holland-Moritz et al. have observed both reversible and irreversible roughening of the Au(111) surface in KCl and a dependence of the surface roughness on the concentration of AgNO<sub>3</sub> and AgClO<sub>4</sub> solutions (F7). Tao and Lindsay have shown that Au(111) reconstructs to the  $\sqrt{3} \times \sqrt{3}$  surface in the presence of H<sub>2</sub>O, HClO<sub>4</sub>, and NaH<sub>2</sub>PO<sub>4</sub> (F8). Weaver and co-workers have also reported atomically-resolved, potential-dependent reconstructions of Au(100) (F9) and Au(111) in aqueous HClO<sub>4</sub> (F10). McCarley and Bard found that dosing Au(111) surface with aqueous KI resulted in a  $3\sqrt{3} \times 3\sqrt{3}$ -R30° adlattice structure (F11).

AFM has been employed to study the disordered oxide on Au(111) in aqueous perchloric acid under potential control (F12) and to obtain atomically resolved images of a Cu monolayer lattice on an Au(111) electrode while under potential control in various electrolyte solutions (F13). Endo et al. imaged the initial stages of island growth for Ag electrodeposited on Au(111) under potential control (F14).

Oppenheim et al. studied surface diffusion in Ag-Au alloys in dilute perchloric acid and discuss their results within the framework of the kink-ledge-terrace model of crystal surfaces and models of alloy corrosion based on percolation theory (F15). The anodic dissolution of Cu from a Cu-Au alloy in the presence and absence of an inhibitor has also been reported and compared to SEM results (F16, F17).

Hoeppner et al. have studied chemically polished macroelectrodes and electrolytically grown microelectrodes in air and under potential control in aqueous solutions. In contrast to the macroelectrodes, the microelectrodes have large atomically flat terraces separated by monoatomic steps. Dynamics of these steps under anodic and cathodic polarization was studied as well as the nucleation and growth of Pb electrodeposited on Ag(111) macroelectrodes (F18). Several authors have discussed the effects of electrochemical oxidation-reduction

cycles on the morphology of Pt(111), Rh(111), and Pd(111), and polycrystalline Al and Fe in aqueous  $H_2SO_4$ , NaOH, borate buffer, and  $HClO_4$  (F19-F22).

Si surfaces have also been imaged under  $H_2SO_4$  with atomic resolution using electrochemical STM under potentiostatic control (F23). Surface roughening during anodic photocorrosion of n-GaAs(100) has also been discussed (F24). The morphology of CdS films deposited on an arachidic acid monolayer, Ti-foil, HOPG, and indium-coated copper were investigated using STM (F25). Sakamaki et al. studied local light-induced structural transformations that occur on the  $MoS_2$ (0001) surface in acetonitrile (F26, F27).

Srinivasan et al. have obtained molecular resolution images of electrochemically condensed layers of guanine on graphite under potential control (F28).

IR reflection-adsorption spectroscopy has been combined with STM to characterize the CO adlayer on Rh(111) in aqueous solutions (F29). Depending on the applied potential, two different structures are obtained corresponding to the  $2 \times 2$ -3CO and  $3 \times \sqrt{3}$  rect-4CO unit cells. The preference for one unit cell over another at a specific applied potential was explained in terms of the extent of  $d\pi-2\pi^*$  metal-CO back-bonding. In situ IR spectroscopy and electrochemical STM have been used to study CO on Pt(100) after replacement of iodine by the CO (F30). In the presence of iodine adlayers, large  $1 \times 1$  terraces are evident; however, upon exposure to aqueous CO the number of smaller  $1 \times 1$  islands increases and coalesces at positive potentials. The results are discussed in terms of the predominance of either bridge-bound or atop-coordinated CO molecules.

Chang et al. have correlated the outer-sphere electron-transfer rates of eight  $Co^{III}(NH_3)_4X$  complexes (where X =  $NH_3$ ,  $F^-$ ,  $OSO_3^{2-}$ ,  $OH^-$ , acetate, and three organic carboxylates) to the spatially resolved adlattice sites in  $\sqrt{7} \times \sqrt{7}$  and  $3 \times 3$  iodine-covered Pt(111) surfaces (F31). Reactants which contain only inorganic ligands have a higher  $k_{app}$  on the  $\sqrt{7} \times \sqrt{7}$  than on the  $3 \times 3$  lattice while those complexes containing aromatic carboxylate ligands show no adlattice preference.

Scanning electrochemical microscopy (SECM), developed by Bard and co-workers, is a scanned-probed microscopy based on measuring the rate of faradaic reactions at the probe tip. Although the spatial resolution of SECM (typically 0.5  $\mu m$  or larger) does not approach that of STM or AFM, the technique has some unique capabilities for investigating the chemical activity and physical properties of heterogeneous surfaces. Bard et al. have reviewed the principles and instrumentation of SECM, as well as applications for fundamental studies of electrodes, minerals, and biological samples (F32). A transient SECM technique has also been reported by the same group that allows measurement of the diffusion coefficient of a redox species in solution, independent of concentration and the number of electrons involved in the reactions (F33). Anson and co-workers have also described SECM imaging of small Pt-disk electrodes (F34).

Scott et al. have employed an SECM to "image" the local molecular flux of electroactive ions across a porous membrane (F35). In this application, the SECM measurement yields the pore structure of the membrane as well as the rate of transport within individual pores.

Several new scanned probe imaging systems were reported during the last year that are based on measuring either the interfacial potential or the local current distribution. Oriani and co-workers reported the use of a Kelvin microprobe to measure the corrosion potential profiles across surfaces of galvanically-coupled metals in humid atmospheres (F36). The same technique was used by Huang et al. to map the work function distribution across thin anodically-grown  $TiO_2$  films (F37). Isaacs et al. have adapted a scanning vibrating probe (VSP) technique (F38) to measure the magnitude and direction of the corrosion current distribution over a steel surface (F39).

## ACKNOWLEDGMENT

STM and SECM investigations in the authors' laboratory are supported by the Office of Naval Research and by the Center for Interfacial Engineering with funding from the NSF Engineering Research Centers Program and industrial sponsors.

## LITERATURE CITED

- (A1) Binnig, G.; Rohrer, H.; Gerber, Ch.; Weibel, E. *Phys Rev Lett* 1982, 49, 57.
- (A2) Ray, M. A.; McGuire, G. E.; Musselman, I. H.; Nemanich, R. J.; Chopra, D. R. *Anal Chem* 1991, 63, 99R-118R.
- (A3) Cooke, P. M. *Anal Chem* 1990, 62, 423R-41R.
- (A4) Chen, J. *J Vac Sci Technol A* 1991, 9, 44-50.
- (A5) *Scanning Tunneling Microscopy and Related Methods*; Behm, R. J.; Garcia, N.; Rohrer, H., Eds.; NATO ASI Series E: Applied Sciences; Kluwer Academic Publishers: Dordrecht, Boston and London, 1990; vol. 184.
- (A6) Binh, V. T.; Garcia, N. *J Phys I* 1991, 1, 605-12.
- (A7) Eng, L. M.; Fuchs, H. *Mater Sci Eng A* 1991, A139, 230-8.
- (A8) Glimzewski, J. K. *NATO ASI Ser C* 1991, 328, 203-15.
- (A9) Metzger, R. M.; Panetta, C. A. *Synth Met* 1991, 42, 1407-13.
- (A10) Lieber, C. M.; Wu, X. L. *Acc Chem Res* 1991, 24, 170-7.
- (A11) Sattler, K. Z. *Phys D* 1991, 19, 287-92.
- (A12) Ehrlich, G. *Surf Sci* 1991, 246, 1-12.
- (A13) Chidsey, C. *Proc—Electrochem Soc (Proc Symp Appl Surf Anal, Methods Environ Mater Interact.)* 1990, 1991, 91, 257-64.
- (A14) Binnig, G.; Quate, C. F.; Gerber, Ch. *Phys Rev Lett* 1986, 56, 930.
- (A15) Sand, D.; Elings, V. J. *J Vac Sci Technol B* 1991, 9, 431-7.
- (B1) Wenzel, M.; Ehinger, M.; Bicknell-Taseau, R. N.; Landwehr, G. *Fresenius J Anal Chem* 1991, 341, 189-92.
- (B2) Fries, T.; Becker, C.; Boshmer, M.; Wandek, K. *Fresenius J Anal Chem* 1991, 341, 193-5.
- (B3) Park, C.; Park, K. S.; Huh, Y. S.; Jeon, I. C.; Kim, S. *J Vac Sci Technol B* 1991, 9, 636-8.
- (B4) Kato, T.; Osaka, F.; Tanaka, I.; Ohkouchi, S. *J Vac Sci Technol B* 1991, 9, 1981-4.
- (B5) Van de Leemput, L. E. C.; Rongen, P. H. H.; Timmerman, B. H.; Van Kempen, H. *Rev Sci Instrum* 1991, 62, 989-92.
- (B6) Sugawara, Y.; Ishizaka, T.; Morita, S. *J Vac Sci Technol B* 1991, 9, 1092-5.
- (B7) Fies-Seiler, L. A.; Randall, J. N.; Harkness, D. *J Vac Sci Technol B* 1991, 9, 659-62.
- (B8) Orr, B. G.; Synder, C. W.; Johnson, M. *Rev Sci Instrum* 1991, 62, 1400-3.
- (B9) Yau, S. L.; Gao, X.; Chang, S. C.; Schardt, B. C.; Weaver, M. J. *J Am Chem Soc* 1991, 113, 8049-56.
- (B10) Moreland, J.; Rice, P. *IEEE Trans Magn* 1991, 27, 1198-201.
- (B11) Moreland, J.; Rice, P. *J Appl Phys* 1991, 70, 520-2.
- (B12) Wiesendanger, R.; Burgler, D.; Tarrach, G.; Wadas, A.; Brodbeck, D.; Quentherodt, H. J.; Guentherodt, G.; Gambino, R. J.; Ruf, R. *J Vac Sci Technol B* 1991, 9, 519-24.
- (B13) First, P. N.; Strosio, J. A.; Pierce, D. T.; Dragoset, R. A.; Celotta, R. J. *J Vac Sci Technol B* 1991, 9, 531-6.
- (B14) Stoll, E. P.; Glimzewski, J. K. *J Vac Sci Technol B* 1991, 9, 843-7.
- (B15) Garcia, C. R.; Huerta Garrica, M. A. *J Vac Sci Technol B* 1991, 9, 870-2.
- (B16) Williams, C. C.; Wickramasinghe, H. K. *J Vac Sci Technol B* 1991, 9, 537-40.
- (B17) Kordic, S.; Van Loenen, E. J.; Walker, A. J. *IEEE Electron Device Lett* 1991, 12, 422-4.
- (B18) Yau, S. T.; Seltz, D.; Nayfeh, M. H. *J Vac Sci Technol B* 1991, 9, 1371-5.
- (B19) Voelcker, M.; Krieger, W.; Walther, H. *Phys Rev Lett* 1991, 66, 1717-20.
- (B20) Voelcker, M.; Krieger, W.; Suzuki, T.; Walther, H. *J Vac Sci Technol B* 1991, 9, 541-4.
- (B21) Grafstrom, S.; Kowalski, J.; Neumann, R.; Probst, O.; Woertge, M. *J Vac Sci Technol B* 1991, 9, 568-72.
- (B22) Ferrel, T. L.; Gouidonnet, J. P.; Reddick, R. C.; Sharp, S. L.; Wermack, R. J. *J Vac Sci Technol B* 1991, 9, 525-30.
- (B23) Gouidonnet, J. P.; Salomon, L.; De Formel, F.; Chebrier, G.; Wermack, R. J.; Ferrel, T. L. *Proc SPIE—Int. Soc. Opt. Eng* 1991, 116-23.
- (B24) Berndt, R.; Schittler, R. R.; Glimzewski, J. K. *J Vac Sci Technol B* 1991, 9, 573-7.
- (B25) Takeuchi, K.; Uehara, Y.; Uehoda, S.; Morita, S. *J Vac Sci Technol B* 1991, 9, 557-60.
- (B26) Smolyaninov, I. I.; Edel'man, V. S.; Zav'yalov, V. V. *Phys Lett A* 1991, 158, 337-40.
- (B27) Jiang, S.; Tomita, N.; Ohsawa, H.; Ohtsu, M. *Jpn J Appl Phys* 1991, 30, 2107-11.
- (B28) Akari, S.; Lux-Steiner, M. C.; Voegt, M.; Stachel, M.; Dransfeld, K. *J Vac Sci Technol B* 1991, 9, 561-3.
- (B29) Kuk, Y.; Becker, R. S.; Silverman, P. J.; Kochanski, G. P. *J Vac Sci Technol B* 1991, 9, 545-50.
- (B30) Oulan, L. Q.; Weesels, B. W. *Appl Phys Lett* 1991, 58, 1295-6.
- (B31) Kazmarek, L. L. *J Vac Sci Technol B* 1991, 9, 1549-56.
- (B32) Alvarado, S. F.; Renaud, P.; Abraham, D. L.; Schoenenberger, C.; Arent, D. J.; Meier, H. P. *J Vac Sci Technol B* 1991, 9, 409-13.
- (B33) Oulan, L. Q.; Weesels, B. W. *Appl Phys Lett* 1991, 58, 2538-9.
- (B34) Adler, J. G.; Chen, T. T.; Gallagher, M. C.; Kontin, M. K.; Mullin, D. P. *J Vac Sci Technol B* 1991, 9, 982-5.
- (B35) Glesl, F. J.; Gerber, C.; Binnig, G. *J Vac Sci Technol B* 1991, 9, 984-8.
- (B36) Cohen, L. F.; Wolf, E. L. *Mesa Sci Technol* 1991, 2, 83-5.
- (B37) Wilkins, R.; Amman, M.; Ben-Jacob, E.; Jaklevic, R. C. *J Vac Sci Technol B* 1991, 9, 996-9.
- (B38) Chen, T.; Tesamer, S.; Tucker, J. R.; Lyding, J. W.; Van Hateringen, D. *J Vac Sci Technol B* 1991, 9, 1000-5.
- (B39) Pan, S.; De Lozanne, A. L.; Fainstein, R. *J Vac Sci Technol B* 1991, 9, 1017-21.

- (B40) Wu, X. L.; Lieber, C. M. *J. Vac. Sci. Technol. B* 1991, 9, 1044-7.
- (B41) Moeller, R.; Baur, C.; Esslinger, A.; Kuerz, P. *J. Vac. Sci. Technol. B* 1991, 9, 608-11.
- (B42) Yaniv, D. R.; McCormick, L. D. *Electroanalysis* 1991, 3, 103-10.
- (B43) Yuan, J. Y.; Shao, Z.; Gao, C. *Phys. Rev. Lett.* 1991, 67, 663-6.
- (B44) Barrett, R. C.; Quate, C. F. *J. Vac. Sci. Technol. B* 1991, 9, 302-6.
- (B45) Miller, G. L.; Griffin, J. E.; Wagner, E. R.; Grigg, D. A. *Rev. Sci. Instrum.* 1991, 62, 705-9.
- (B46) Den Boef, A. *J. Vac. Sci. Technol. B* 1991, 9, 88-92.
- (B47) Fujii, T.; Suzuki, M.; Miyashita, M.; Yamaguchi, M.; Onuki, T.; Nakamura, H.; Matsubara, T.; Yamada, H.; Nakayama, K. *J. Vac. Sci. Technol. B* 1991, 9, 666-9.
- (B48) Barrett, R. C.; Quate, C. F. *Rev. Sci. Instrum.* 1991, 62, 1393-9.
- (B49) Weaver, J. M. R.; Wickramasinghe, H. K. *J. Vac. Sci. Technol. B* 1991, 9, 1562-5.
- (B50) Weaver, J. M. R.; Abraham, D. W. *J. Vac. Sci. Technol. B* 1991, 9, 1559-61.
- (B51) Denk, W.; Pohl, D. W. *Appl. Phys. Lett.* 1991, 59, 2171-3.
- (B52) Barrett, R. C.; Quate, C. F. *J. Appl. Phys.* 1991, 70, 2725-33.
- (B53) Abraham, D. W.; Williams, C.; Slinkman, J.; Wickramasinghe, H. K. *J. Vac. Sci. Technol. B* 1991, 9, 703-6.
- (B54) Nishikawa, O.; Tomitori, M.; Iwawaki, F. *Mater. Sci. Eng.* 1991, 88, 81-97.
- (B55) Liowaki, W.; Van den Berg, A. H. J.; Kip, G. A. M.; Hanekamp, L. J. *Fresenius' J. Anal. Chem.* 1991, 341, 196-9.
- (B56) Nishikawa, O.; Koyama, H.; Tomitori, M.; Iwawaki, F. *J. Vac. Sci. Technol. B* 1991, 9, 789-93.
- (B57) Venkateswaran, N.; Sattler, K.; Müller, U.; Kaiser, B.; Raina, G.; Xhie, J. *J. Vac. Sci. Technol. B* 1991, 9, 1052-4.
- (B58) Ikebe, S.; Shimada, D.; Akahane, T.; Tsuda, N. *Jpn. J. Appl. Phys.* 1991, 30, L405-6.
- (B59) Nonnenmacher, M.; Greshner, J.; Wotter, O.; Kassing, R. *J. Vac. Sci. Technol. B* 1991, 9, 1358-62.
- (B60) Wotter, O.; Bayer, T.; Greshner, J. *J. Vac. Sci. Technol. B* 1991, 9, 1353-7.
- (B61) Hellmans, L.; Weysert, K.; Hennau, F.; Stockman, L.; Heyvaert, I.; Van Haesendonck, C. *J. Vac. Sci. Technol. B* 1991, 9, 1309-12.
- (B62) Dreider, K. E. *J. Vac. Sci. Technol. B* 1991, 9, 1394-7.
- (C1) Womeladorf, J. F.; Sawamura, M.; Ermler, W. C. *Surf. Sci.* 1991, 241, L11-5.
- (C2) Ishiki, N.; Kobayashi, K.; Tsukada, M. *J. Vac. Sci. Technol. B* 1991, 9, 475-8.
- (C3) Tsukada, M.; Kobayashi, K.; Ishiki, N. *Surf. Sci.* 1991, 242, 12-7.
- (C4) Landman, U.; Luedtke, W. D. *J. Vac. Sci. Technol. B* 1991, 9, 414-23.
- (C5) Chen, C. J.; Hamers, R. J. *J. Vac. Sci. Technol. B* 1991, 9, 503-5.
- (C6) Huang, Z. H.; Weimer, M.; Allen, R. E. *J. Vac. Sci. Technol. B* 1991, 9, 2399-404.
- (C7) Echanique, P. M.; Uranga, M. E. *Surf. Sci.* 1991, 247, 125-32.
- (C8) Garcia-Garcia, R.; Jose Saez, J. *Surf. Sci.* 1991, 251-252, 223-7.
- (C9) Garcia-Garcia, R.; Garcia, N. *Surf. Sci.* 1991, 251-252, 408-12.
- (C10) Garcia, R. *J. Vac. Sci. Technol. B* 1991, 9, 500-2.
- (C11) Denk, W.; Pohl, D. W. *J. Vac. Sci. Technol. B* 1991, 9, 510-3.
- (C12) Sasa, J. K.; Gimzewski, J. K. *J. Electroanal. Chem. Interfacial Electrochem.* 1991, 308, 333-7.
- (C13) Coley, T. R.; Goddard, W. A., III; Baldeeschweiler, J. D. *J. Vac. Sci. Technol. B* 1991, 9, 470-4.
- (C14) Batista, I.; Gammel, J. T.; Bishop, A. R. *Synth. Met.* 1991, 42, 2727-32.
- (C15) Sauer, P.; Joachim, C. *Chem. Phys. Lett.* 1991, 185, 23-30.
- (C16) Joachim, C. *New J. Chem.* 1991, 15, 223-9.
- (C17) Lazzaroni, R.; Calderone, A.; Lambin, G.; Rabe, J. P.; Bredas, J. L. *Synth. Met.* 1991, 41, 525-8.
- (C18) Ding, Y. G.; Chen, C. T.; Ho, K. M. *Phys. Rev. Lett.* 1991, 67, 1454-7.
- (C19) Watanabe, S.; Aono, M.; Tsukada, M. *Phys. Rev. B* 1991, 44, 8330-3.
- (C20) Karlotta, R.; Lagally, M. G. *Surf. Sci.* 1991, 248, 295-305.
- (C21) Holander, J. M.; Jedrzak, C. *Acta Phys. Pol. A* 1991, 79, 117-20.
- (C22) Badziag, P.; Verwoerd, W. S.; Van Hove, M. A. *Phys. Rev. B* 1991, 43, 2058-62.
- (C23) Tanaka, Y.; Tsukada, M. *Solid State Commun.* 1991, 77, 593-6.
- (C24) Howell, S.; Chen, T.; Gallagher, M.; Yi, L.; Sarid, D. *J. Appl. Phys.* 1991, 69, 7330-2.
- (C25) Girard, C.; Bouji, X. *J. Chem. Phys.* 1991, 95, 2056-64.
- (C26) Maghazzi, S.; Girard, C.; Van Labak, D. *J. Phys. I* 1991, 1, 289-307.
- (C27) Hartmann, U. *J. Vac. Sci. Technol. B* 1991, 9, 465-9.
- (C28) Girard, C.; Maghazzi, S. *Surf. Sci.* 1991, 255, L571-8.
- (C29) Duckler, W. A.; Sonden, T. J.; Pashley, R. M. *Nature (London)* 1991, 353, 236-41.
- (C30) Krantzman, K. D.; Rees, D. C.; Farnely, D. J. *Phys. Chem.* 1991, 95, 9039-42.
- (C31) Tomanek, D.; Zhong, W. *Phys. Rev. B* 1991, 43, 12623-5.
- (C32) Tomanek, D.; Zhong, W.; Thomas, H. *Europhys. Lett.* 1991, 15, 887-92.
- (C33) Zhong, W.; Overmyer, G.; Tomanek, D. *Europhys. Lett.* 1991, 15, 48-54.
- (C34) Forcada, M. L.; Jakas, M. M.; Grae-Marti, A. *J. Chem. Phys.* 1991, 95, 706-8.
- (D1) Chambliss, D. D.; Wilson, R. J. *J. Vac. Sci. Technol. B* 1991, 9, 926-32.
- (D2) Chambliss, D. D.; Wilson, R. J.; Chiang, S. *Phys. Rev. Lett.* 1991, 66, 1721-4.
- (D3) Chambliss, D. D.; Wilson, R. J.; Chiang, S. *J. Vac. Sci. Technol. B* 1991, 9, 833-7.
- (D4) Voigtlander, B.; Meyer, G. *Amer. N. M. Surf. Sci.* 1991, 255, L529-35.
- (D5) Nichols, R. J.; Kolb, D. M.; Behm, R. J. *J. Electroanal. Chem. Interfacial Electrochem.* 1991, 313, 109-19.
- (D6) Magnussen, O. M.; Hodges, J.; Beitel, G.; Kolb, D. M.; Behm, R. J. *J. Vac. Sci. Technol. B* 1991, 9, 989-75.
- (D7) Poetschke, G. O.; Behm, R. J. *Phys. Rev. B* 1991, 44, 1442-5.
- (D8) Poetschke, G.; Schroeder, J.; Guenther, C.; Hwang, R. Q.; Behm, R. J. *Surf. Sci.* 1991, 251-252, 592-6.
- (D9) Schleicher, B.; Jung, T.; Mug, H.; Bartscher, H. *Z. Phys. D* 1991, 19, 327-31.
- (D10) Nishitani, R.; Kasuya, A.; Kubota, S.; Nishina, Y. *J. Vac. Sci. Technol. B* 1991, 9, 806-9.
- (D11) Nishitani, R.; Kasuya, A.; Kubota, S.; Nishina, Y. *Z. Phys. D* 1991, 19, 333-5.
- (D12) Womeladorf, J. F.; Ermler, W. C.; Sandrof, C. *J. Phys. Chem.* 1991, 95, 503-5.
- (D13) Becker, C.; Fries, T.; Wendel, K.; Kretzig, U.; Schmid, G. *J. Vac. Sci. Technol. B* 1991, 9, 810-3.
- (D14) Van de Leemput, L. E. C.; Gerritsen, J. W.; Rongan, P. H. H.; Smokers, R. T. M.; Wieringa, H. A.; Van Kampen, H.; Schmid, G. *J. Vac. Sci. Technol. B* 1991, 9, 814-9.
- (D15) Strong, L.; Evans, D. F.; Gladfelter, W. L. *Langmuir* 1991, 7, 442-3.
- (D16) Kojima, I.; Srivastava, A. K.; Kurahashi, M. *Jpn. J. Appl. Phys.* 1991, 30, 1852-3.
- (D17) Siperko, L. M. *J. Vac. Sci. Technol. B* 1991, 9, 1457-60.
- (D18) Kennedy, R. M.; Minton, K.; Yang, X.; Evans, D. F. *J. Vac. Sci. Technol. B* 1991, 9, 735-6.
- (D19) Yeung, K. L.; Wolf, E. E. *J. Vac. Sci. Technol. B* 1991, 9, 798-803.
- (D20) Zhou, X. C.; Gulari, E. *Acta Crystallogr.* 1991, A47, 17-21.
- (D21) Xhie, J.; Sattler, K.; Müller, U.; Venkateswaran, N.; Raina, G. *Phys. Rev. B* 1991, 43, 8917-23.
- (D22) Xhie, J.; Sattler, K.; Müller, U.; Venkateswaran, N.; Raina, G. *J. Vac. Sci. Technol. B* 1991, 9, 833-6.
- (D23) Brewer, P. J.; Geesey, G. G.; Drake, B.; Jolley, J. G.; Harkins, M. R. *Surf. Interface Anal.* 1991, 17, 767-72.
- (D24) LeBale, F. M.; Hirschorn, E. S.; Samsavar, A.; Miller, T.; Chiang, T. C. *Phys. Rev. B* 1991, 44, 8115-20.
- (D25) Krausch, G.; Detzel, T.; Bleisfeld, H.; Fink, R.; Luckscheiter, B.; Platzer, R.; Wochmann, U.; Schatz, G. *Appl. Phys. A* 1991, A53, 324-9.
- (D26) Yang, Y. N.; Trafas, B. M.; Luo, Y. S.; Siefert, R. L.; Weaver, J. H. *Phys. Rev. B* 1991, 44, 5720-5.
- (D27) Trafas, B. M.; Yang, Y. N.; Siefert, R. L.; Weaver, J. H. *Phys. Rev. B* 1991, 43, 14107-14.
- (D28) Trafas, B. M.; Hill, D. M.; Benning, P. J.; Waddell, G. D.; Yang, Y. N.; Siefert, R. L.; Weaver, J. H. *Phys. Rev. B* 1991, 43, 7174-84.
- (D29) Phoner, M.; Stromadoerfer, G.; Li, Y. W.; Martin, J. R.; De Villeneuve, C.; Porte, L. J. *Electrochem. Soc.* 1991, 138, 874-5.
- (D30) Suzuki, M.; Fukuda, T. *Phys. Rev. B* 1991, 44, 3187-90.
- (D31) England, C. D.; Engel, B. N.; Falco, C. M. *J. Appl. Phys.* 1991, 69, 5310-2.
- (D32) Baur, E. *Surf. Sci.* 1991, 250, L379-82.
- (D33) Hasegawa, T.; Takata, K.; Hosaka, S.; Hosok, S. *J. Vac. Sci. Technol. B* 1991, 9, 758-60.
- (D34) Gartz, E.; Xiong, F.; Hwang, I. S.; Golovchenko, J. *Phys. Rev. B* 1991, 43, 7316-9.
- (D35) Nogami, J.; Beak, A. A.; Quate, C. F. *Phys. Rev. B* 1991, 44, 1415-8.
- (D36) Hanabusa, M.; Sahara, K. *Mater. Res. Soc. Symp. Proc.* 1991, 201, 607-12.
- (D37) Sahara, K.; Ouchi, H.; Hanabusa, M. *Jpn. J. Appl. Phys.* 1991, 30, 1548-8.
- (D38) Haseizume, T.; Hasegawa, Y.; Sekurai, T. *Appl. Surf. Sci.* 1991, 48-49, 119-24.
- (D39) Haseizume, T.; Hasegawa, Y.; Sumita, I.; Sekurai, T. *Surf. Sci.* 1991, 246, 189-94.
- (D40) Haseizume, T.; Sumita, I.; Murata, Y.; Hyodo, S.; Sekurai, T. *J. Vac. Sci. Technol. B* 1991, 9, 742-4.
- (D41) Haseizume, T.; Motai, K.; Hasegawa, Y.; Sumita, I.; Tanaka, H.; Arano, S.; Hyodo, S.; Sekurai, T. *J. Vac. Sci. Technol. B* 1991, 9, 745-7.
- (D42) Betra, I. P. *Phys. Rev. B* 1991, 43, 12232-34.
- (D43) Blawie, H. B.; Dijkamp, D.; Van Loenen, E. J. *Phys. Rev. B* 1991, 44, 3802-9.
- (D44) Nogami, J.; Geald, A. A.; Quate, C. F. *Appl. Phys. Lett.* 1991, 58, 475-7.
- (D45) Richter, M.; Wolck, J. C.; Planeta, P.; Miyano, K. E.; Kondelewicz, T.; Boudin, C. E.; Spicer, W. E.; Lindau, I. *J. Vac. Sci. Technol. A* 1991, 9, 1951-5.
- (D46) Richter, M.; Wolck, J. C.; Nogami, J.; Planeta, P.; Miyano, K. E.; Beak, A. A.; Kondelewicz, T.; Boudin, C. E.; Spicer, W. E. *Phys. Rev. Lett.* 1991, 66, 2636.
- (D47) Beak, A. A.; Nogami, J.; Quate, C. F. *Phys. Rev. B* 1991, 43, 8316-9.
- (D48) Beak, A. A.; Nogami, J.; Quate, C. F. *J. Vac. Sci. Technol. A* 1991, 9, 1946-50.
- (D49) Whitman, L. J.; Stroscio, J. A.; Dragoset, R. A.; Celotta, R. *J. Phys. Rev. B* 1991, 44, 5951-4.
- (D50) Whitman, L. J.; Stroscio, J. A.; Dragoset, R. A.; Celotta, R. *J. Phys. Rev. Lett.* 1991, 66, 1338-41.
- (D51) Li, Y. Z.; Patrin, J. C.; Chen, Y.; Weaver, J. H. *Phys. Rev. B* 1991, 44, 8843-9.
- (D52) Komada, T.; Anderson, S. G.; Seo, J. M.; Schabel, M. C.; Weaver, J. H. *J. Vac. Sci. Technol. B* 1991, 9, 1904-71.
- (D53) Barkovits, V. L.; Besolov, V. N.; Lvova, T. V.; Makarenko, I. V.; Safarov, V. I.; Tsarenkov, B. V. *Mater. Sci. Eng. B* 1991, 9, 43-6.
- (D54) Allan, G.; Lannoo, M. *Phys. Rev. Lett.* 1991, 66, 1208-11.

- (D55) DeRose, J. A.; Thundat, T.; Nagahara, L. A.; Lindsay, S. M. *Surf. Sci.* 1991, 256, 102-8.
- (D56) Rebe, J. P.; Buchholz, S. *Appl. Phys. Lett.* 1991, 58, 702-4.
- (D57) Colchero, J.; Martí, O.; Mlynik, J.; Humbert, A.; Henry, C. R.; Chapon, C. *J. Vac. Sci. Technol. B* 1991, 9, 794-7.
- (D58) Buchholz, S.; Fuchs, H.; Rebe, J. P. *J. Vac. Sci. Technol. B* 1991, 9, 857-81.
- (D59) Mazur, U.; Fried, G.; Hips, K. W. *Surf. Sci.* 1991, 9, 179-92.
- (D60) Dawson, P.; Alexander, K. B.; Thompson, J. R.; Haas, J. W.; Ferrel, T. *Phys. Rev. B* 1991, 44, 6372-81.
- (D61) Yamada, I.; Takahata, G. H.; Ueda, H.; Satoh, F.; Itoh, Y.; Yamaoka, K.; Kitamoto, S.; Namba, Y.; Hashimoto, Y. *Nucl. Instrum. Methods Phys. Res.* 1991, B55, 878-9.
- (D62) Bartlett, R.; Jaeger, H.; Sexton, B. A.; Netterfield, R. P.; Martin, P. J. *Appl. Surf. Sci.* 1991, 47, 187-91.
- (D63) Weisenhorn, A. L.; Henriksen, P. N.; Chu, H. T.; Ramaker, R. D.; Reneker, D. H. *J. Vac. Sci. Technol. B* 1991, 9, 1333-5.
- (D64) Meyer, J. A.; Kuk, Y.; Estrup, P. J.; Silverman, P. J. *Phys. Rev. B* 1991, 44, 9104-7.
- (D65) Kopatzki, E.; Behm, R. J. *Surf. Sci.* 1991, 245, 255-82.
- (D66) Haase, O.; Koch, R.; Borbonus, M.; Rieder, K. H. *Phys. Rev. Lett.* 1991, 66, 1725-8.
- (D67) Baeumer, M.; Cappus, D.; Kuhlbeck, H.; Freund, H. J.; Wilhelm, G.; Brodde, A.; Naddermeyer, H. *Surf. Sci.* 1991, 253, 116-28.
- (D68) Besenbacher, F.; Jensen, F.; Laegsgaard, E.; Mortensen, K.; Stenagaard, I. *J. Vac. Sci. Technol. B* 1991, 9, 874-8.
- (D69) Kern, K.; Niehus, H.; Schatz, A.; Zeppenfeld, P.; George, J.; Comsa, G. *Phys. Rev. Lett.* 1991, 67, 855-8.
- (D70) Wintterlin, J.; Schuster, R.; Coulman, D. J.; Ertl, G.; Behm, R. J. *J. Vac. Sci. Technol. B* 1991, 9, 902-8.
- (D71) Hanzhurne, T.; Taniguchi, M.; Motai, K.; Lu, H.; Tanaka, K.; Sakurai, T. *Jpn. J. Appl. Phys.* 1991, 30, L1529-31.
- (D72) Niehus, H.; Spitzel, R.; Besocke, K.; Comsa, G. *Phys. Rev. B* 1991, 43, 12619-22.
- (D73) Schuster, R.; Barth, J. V.; Ertl, G.; Behm, R. J. *Surf. Sci.* 1991, 247, L229-34.
- (D74) Ogletree, D. F.; Hwang, R. Q.; Zaglinski, D. M.; Lopez, V. A.; Somorjai, G. A.; Salmeron, M. *J. Vac. Sci. Technol. B* 1991, 9, 886-90.
- (D75) Hwang, R. Q.; Zaglinski, D. M.; Lopez, V. A.; Ogletree, D. F.; Somorjai, G. A.; Salmeron, M.; Denary, D. R. *Phys. Rev. B* 1991, 44, 1914-7.
- (D76) Roberts, C. J.; Hoffmann-Millack, B.; Steer, W. S. *J. Vac. Sci. Technol. B* 1991, 9, 841-4.
- (D77) Haase, W.; Lackey, D.; Sass, J. K. *J. Chem. Phys.* 1991, 95, 2193-6.
- (D78) Gmzewski, J. K.; Berndt, R.; Schüttler, R. R. *Surf. Sci.* 1991, 247, 327-32.
- (D79) Gmzewski, J. K.; Berndt, R.; Schüttler, R. R. *J. Vac. Sci. Technol. B* 1991, 9, 897-901.
- (D80) Borbonus, M.; Koch, R.; Haase, O.; Rieder, K. H. *Surf. Sci.* 1991, 249, L317-21.
- (D81) Michely, T.; Comsa, G. *J. Vac. Sci. Technol. B* 1991, 9, 882-6.
- (D82) Stephan, R.; Gaertner, H.; Rueck, D. M. *GSI-Rep.* 1991, 91, 243.
- (D83) Michely, T.; Comsa, G. *Surf. Sci.* 1991, 250 (3), 217-26.
- (D84) Lang, C. A.; Quate, C. F.; Nogami, J. *Appl. Phys. Lett.* 1991, 59, 1696-8.
- (D85) Tench, R. J.; Balooch, M.; Bernardaz, L.; Allen, M. J.; Siskhaus, W. J.; Olander, D. R.; Wang, W. *J. Vac. Sci. Technol. B* 1991, 9, 820-4.
- (D86) Scandella, L.; Stauffer, U.; Brodbeck, D.; Reimann, P.; Guentherodt, H. J.; Zehring, R.; Heuert, R.; Moser, E. M. *Mater. Sci. Eng.* 1991, A133, 601-5.
- (D87) Heilen, H. D.; Fernandez, A.; Huang, T.; Buhman, R. A.; Sisco, J. J. *J. Vac. Sci. Technol. B* 1991, 9, 885-90.
- (D88) Schowalter, L. J.; Lee, E. Y. *Phys. Rev. B* 1991, 43, 9306-11.
- (D89) Ludtke, R.; Pritsch, M.; Sarnavver, A. *J. Vac. Sci. Technol. B* 1991, 9, 2342-8.
- (D90) Ohmori, T.; Sakamaki, K.; Hashimoto, K.; Fujihira, A. *Chem. Lett.* 1991, 7, 93-6.
- (D91) Besenbacher, F.; Laegsgaard, E.; Stenagaard, I.; Stoltze, P.; Topsoe, H. *Catal. Lett.* 1991, 6, 273-82.
- (D92) KeKoven, B. M.; Mayers, G. F. *J. Vac. Sci. Technol. A* 1991, 9, 2570-7.
- (D93) Endo, T.; Yamada, H.; Sumomogi, T.; Kuwahara, K.; Morita, S. *J. Vac. Sci. Technol. B* 1991, 9, 837-40.
- (D94) Rice, P.; Moreland, J. *Rev. Sci. Instrum.* 1991, 62, 844-5.
- (D95) Tang, S. L.; Carola, P. F.; McChie, A. J.; James, E. B. *Appl. Phys. Lett.* 1991, 59, 288-91.
- (D96) Wolf, J. F.; Ibach, H. *Appl. Phys. A* 1991, A52, 218-21.
- (D97) Everson, M. P.; Davis, L. C.; Jaklevic, R. C.; Shen, W. *J. Vac. Sci. Technol. B* 1991, 9, 891-6.
- (D98) Gomez-Rodriguez, J. M.; Bero, A. M.; Salverezza, R. C. *J. Vac. Sci. Technol. B* 1991, 9, 496-9.
- (D99) Lanford, J.; Longmire, M. *J. Mater. Sci.* 1991, 26, 1131-6.
- (D100) Komarica, S.; Kopp, W. U. *Sonderb. Prakt. Metallogr.* 1991, 22, 281-91.
- (D101) Moeller, R.; Albrecht, U.; Boneberg, J.; Koslowski, B.; Lelander, P.; Oranfeld, K. *J. Vac. Sci. Technol. B* 1991, 9, 907-9.
- (D102) Smolyaninov, I. I.; Edelman, V. S.; Zav'yalov, V. V. *Phys. Lett. A* 1991, 158, 337-40.
- (D103) Takahashi, K.; Uehara, Y.; Ushida, S.; Morita, S. *J. Vac. Sci. Technol. B* 1991, 9, 857-60.
- (D104) Fan, F. R.; Bard, A. J. *J. Phys. Chem.* 1991, 95, 1966-76.
- (D105) Kazmerak, L. L. *J. Vac. Sci. Technol. B* 1991, 9, 1549-56.
- (D106) Zhao, X. K.; McCormick, L. D.; Fendler, J. H. *Langmuir* 1991, 7, 1255-60.
- (D107) Zhao, X. K.; Fendler, J. H. *J. Phys. Chem.* 1991, 95, 3716-23.
- (D108) Zhao, X. K.; Fendler, J. H. *Chem. Mater.* 1991, 3, 166-74.
- (D109) Feenstra, R. M.; Lutz, M. A. *Surf. Sci.* 1991, 243, 151-65.
- (D110) Feenstra, R. M.; Lutz, M. A. *J. Vac. Sci. Technol. B* 1991, 9, 716-20.
- (D111) Ancillotto, F.; Selloni, A.; Tosatti, E. *Phys. Rev. B* 1991, 43, 14726-9.
- (D112) Tsukada, M.; Kobayashi, K.; Shima, N.; Ishiki, N. *J. Vac. Sci. Technol. B* 1991, 9, 492-4.
- (D113) Kitamura, S.; Sato, Y.; Iwatsuki, M. *Nature* 1991, 351, 215-7.
- (D114) Terrach, G.; Wiesendanger, R.; Buegler, D.; Scandella, L.; Guentherodt, H. *J. Vac. Sci. Technol. B* 1991, 9, 877-80.
- (D115) Kneil, J.; Pathica, J. B.; Todd, J. D.; Wilson, J. H. *Phys. Rev. Lett.* 1991, 66, 1733-6.
- (D116) Sugihara, K.; Sakai, A.; Kato, Y.; Akama, Y.; Shoda, N.; Tokumoto, H.; Ono, M. *J. Vac. Sci. Technol. B* 1991, 9, 707-10.
- (D117) Kochanski, G. P.; Griffin, J. E. *Surf. Sci.* 1991, 249, L293-9.
- (D118) Brooks, G.; Kelly, P. J.; Car, R. C. *Phys. Rev. Lett.* 1991, 66, 1729-32.
- (D119) LaBrecque, J. V.; Cheaman, R. C.; McGuire, G. E.; Nemanich, R. J. *J. Vac. Sci. Technol. B* 1991, 9, 752-7.
- (D120) Kardic, S.; Van Loenen, E. J.; Walker, A. *J. IEEE Electron Device Lett.* 1991, 12, 422-4.
- (D121) Heesal, H. E.; Mammart, U.; Cervi, H.; Behm, R. *J. Vac. Sci. Technol. B* 1991, 9, 690-4.
- (D122) Takigami, T.; Tanimoto, M. *Appl. Phys. Lett.* 1991, 58, 2288-90.
- (D123) Kuk, Y.; Becker, R. S.; Silverman, P. J.; Kochanski, G. P. *J. Vac. Sci. Technol. B* 1991, 9, 545-60.
- (D124) Cahill, D. G.; Hamers, R. J. *J. Vac. Sci. Technol. B* 1991, 9, 564-7.
- (D125) Oulan, L. Q.; Wessels, B. W. *Appl. Phys. Lett.* 1991, 58, 1295-8.
- (D126) Boland, J. J. *Phys. Rev. Lett.* 1991, 67, 1539-42.
- (D127) Wu, C. J.; Carter, E. A. *Chem. Phys. Lett.* 1991, 185, 172-6.
- (D128) Boland, J. J. *Phys. Rev. B* 1991, 44, 1383-6.
- (D129) Mortensen, K.; Chen, D. M.; Badroozan, P. J.; Golovchenko, J. A.; Besenbacher, F. *Phys. Rev. B* 1991, 43, 1816-9.
- (D130) Boland, J. J. *J. Phys. Chem.* 1991, 95, 1521-4.
- (D131) Boland, J. J. *Surf. Sci.* 1991, 244, 1-14.
- (D132) Boland, J. J. *J. Vac. Sci. Technol. B* 1991, 9, 764-9.
- (D133) Morita, Y.; Miki, K.; Tokumoto, H. *Appl. Phys. Lett.* 1991, 59, 1347-9.
- (D134) Kim, Y.; Lieber, C. M. *J. Am. Chem. Soc.* 1991, 113, 2333-5.
- (D135) Higashi, G. S.; Becker, R. S.; Chabal, Y. J.; Becker, A. *J. Appl. Phys.* 1991, 59, 1656-8.
- (D136) Carrojo, J. P.; Thundat, T.; Nagahara, L. A.; Lindsay, S. M.; Majumdar, A. *J. Vac. Sci. Technol. B* 1991, 9, 955-9.
- (D137) Avouris, P.; Lyo, I. W.; Bozso, F. *J. Vac. Sci. Technol. B* 1991, 9, 424-30.
- (D138) Avouris, P.; Lyo, I. W. *Surf. Sci.* 1991, 242, 1-11.
- (D139) Peiz, J. P.; Koch, R. H. *J. Vac. Sci. Technol. B* 1991, 9, 775-8.
- (D140) Kobayashi, Y.; Sugii, K. *J. Vac. Sci. Technol. B* 1991, 9, 748-51.
- (D141) Tabe, M.; Tanimoto, M. *Appl. Phys. Lett.* 1991, 58, 2105-7.
- (D142) Hadley, M. J.; Teer, S. P. *Surf. Sci.* 1991, 247, L221-3.
- (D143) Wei, J.; Wang, X. S.; Bartlett, N. C.; Williams, E. D.; Tung, R. T. *J. Chem. Phys.* 1991, 94, 8384-9.
- (D144) Edelman, V. S.; Fiorova, L. K.; Polyak, L. E.; Stepanyan, G. A.; Vozdn, A. P.; Stepanov, E. A. *Phys. Status Solidi A* 1991, 123, 193-9.
- (D145) Iwawaki, F.; Tomitori, M.; Nishikawa, O. *J. Vac. Sci. Technol. B* 1991, 9, 711-5.
- (D146) Umbach, C. C.; Keffe, M. E.; Blakely, J. M. *J. Vac. Sci. Technol. B* 1991, 9, 721-5.
- (D147) Tokumoto, H.; Wakiyama, S.; Miki, K.; Murakami, H.; Okayama, S.; Kitamura, K. *J. Vac. Sci. Technol. B* 1991, 9, 695-8.
- (D148) Goldberg, J. L.; Wang, X. S.; Wei, J.; Bartlett, N. C.; Williams, E. D. *J. Vac. Sci. Technol. B* 1991, 9, 1866-73.
- (D149) Goldberg, J. L.; Wang, X. S.; Bartlett, N. C.; Williams, E. D. *Surf. Sci.* 1991, 249, L285-92.
- (D150) Umbach, C. C.; Keffe, M. E.; Blakely, J. M. *J. Vac. Sci. Technol. A* 1991, 9, 1014-9.
- (D151) Tokumoto, H.; Miki, K.; Murakami, H.; Kitamura, K. *J. Vac. Sci. Technol. B* 1991, 9, 696-702.
- (D152) Webb, M. B.; Men, F. K.; Swartzentruber, B. S.; Karlots, R.; Legally, M. G. *Surf. Sci.* 1991, 242, 23-31.
- (D153) Yamaguchi, T.; Fujima, M. *J. Phys. Soc. Jpn.* 1991, 60, 1028-39.
- (D154) Yamaguchi, T.; Fujima, N. *Surf. Sci.* 1991, 242, 233-8.
- (D155) Ancillotto, F.; Selloni, A.; Tosatti, E. *Phys. Rev. B* 1991, 43, 5180-3.
- (D156) Karlots, R. *Surf. Sci.* 1991, 248, 306-12.
- (D157) Hartmann, E.; Hahn, P. O.; Behm, R. *J. Appl. Phys.* 1991, 69, 4273-81.
- (D158) Koshler, U.; Justo, O.; Pritsch, G.; Mueller, B.; Hender, M. *Surf. Sci.* 1991, 248, 321-31.
- (D159) Iwawaki, F.; Tomitori, M.; Nishikawa, O. *Surf. Sci.* 1991, 253, L411-6.
- (D160) Mo, Y. W.; Legally, M. G. *Surf. Sci.* 1991, 248, 313-20.
- (D161) Mo, Y. W.; Legally, M. G. *J. Cryst. Growth* 1991, 111, 676-81.
- (D162) Alvarez, J.; Hinerjaps, J. J.; Michel, E. G.; Gallego, J. M.; Vazquez de Parga, A. L.; De la Figuera, J.; Ocal, C.; Miranda, R. *Appl. Phys. Lett.* 1991, 5, 99-101.
- (D163) Klamer, T.; Becker, R. S.; Victors, J. S. *Phys. Rev. B* 1991, 44, 1817-24.
- (D164) Hirschorn, E. S.; Lin, D. S.; Leibels, F. M.; Sarnavver, A.; Chiang, T. C. *Phys. Rev. B* 1991, 44, 1403-8.
- (D165) Feenstra, R. M.; Slavin, A. J. *Surf. Sci.* 1991, 251-2, 401-7.
- (D166) Feenstra, R. M.; Slavin, A. J.; Held, G. A.; Lutz, M. A. *Phys. Rev. Lett.* 1991, 66, 3267-60.
- (D167) Varhus, W. J.; Carull, J. M.; Miller, J. A.; Peterson, G. G. *J. Vac. Sci. Technol. B* 1991, 9, 2022-6.
- (D168) Tanaka, I.; Ohkouchi, S. *Jpn. J. Appl. Phys.* 1991, 30, L1662-4.
- (D169) Snyder, C. W.; Bartlett, D.; Orr, B. G.; Bhattacharya, P. K.; Singh, J. *J. Vac. Sci. Technol. B* 1991, 9, 2189-93.

- (D170) Snyder, C. W.; Orr, B. G.; Kessler, D.; Sander, L. M. *Phys. Rev. Lett.* 1991, 66, 3032-5.
- (D171) Numura, T.; Murakami, K.; Ishikawa, K.; Miyao, M.; Yamaguchi, T.; Sasaki, A.; Hagino, M. *Surf. Sci.* 1991, 242, 166-70.
- (D172) Pedio, M.; Grazia Betti, M.; Ottaviani, C.; Quaresima, C.; Capozzi, M. *Phys. Rev. B* 1991, 43, 9070-5.
- (D173) Prietsch, M.; Samsavar, A.; Ludeke, R. *Phys. Rev. B* 1991, 43, 11850-6.
- (D174) Bringans, R. O.; Siegleisen, O. K.; Swartz, L. E. *Phys. Rev. B* 1991, 44, 3054-63.
- (D175) Kato, T.; Osaka, F. *Jpn. J. Appl. Phys.* 1991, 40, L1586-7.
- (D176) Kato, T.; Osaka, F.; Tanaka, I.; Ohkouchi, S. *J. Vac. Sci. Technol. B* 1991, 9, 1981-4.
- (D177) Kato, T.; Osaka, F.; Tanaka, I.; Ohkouchi, S. *AIP Conf. Proc.* 1991, 227, 64-7.
- (D178) Salemink, H.; Albrektsen, O. *J. Vac. Sci. Technol. B* 1991, 9, 779-82.
- (D179) Albrektsen, O.; Koensraad, P.; Salemink, H. *Proc. SPIE—Int. Soc. Opt. Eng.* 1991, 1367, 336-42.
- (D180) Weiner, J. S.; Hess, H. F.; Robinson, R. B.; Hayes, T. R.; Silco, D. L.; Cho, A. Y.; Ranada, M. *Appl. Phys. Lett.* 1991, 58, 2402-4.
- (D181) Renaud, P.; Alvarado, S. F. *Phys. Rev. B* 1991, 44, 6340-3.
- (D182) Albrektsen, O.; Alvarado, S. F.; Meier, H. P.; Renaud, P.; Salemink, H. W. M. *AIP Conf. Proc.* 1991, 227, 60-3.
- (D183) Alvarado, S. F.; Renaud, P.; Abraham, D. L.; Schoonenberger, C.; Arent, D. J.; Meier, H. P. *J. Vac. Sci. Technol. B* 1991, 9, 409-13.
- (D184) Tanaka, I.; Ohkouchi, S.; Kato, T.; Osaka, F. *J. Vac. Sci. Technol. B* 1991, 9, 2277.
- (D185) Pashley, M. D.; Haberern, K. W.; Gaines, J. M. *J. Vac. Sci. Technol. B* 1991, 9, 938-43.
- (D186) Pashley, M. D.; Haberern, K. W.; Gaines, J. M. *Appl. Phys. Lett.* 1991, 58, 406-8.
- (D187) Ohkouchi, S.; Tanaka, I. *Jpn. J. Appl. Phys.* 1991, 30, L1826-9.
- (D188) McCoy, J. M.; McKay, P. A. *J. Cryst. Growth* 1991, 111, 178-83.
- (D189) Cox, G.; Szyntka, D.; Poppe, U.; Graf, K. H.; Urban, K.; Kisielowski-Kammerich, C.; Krueger, J.; Alexander, H. *J. Vac. Sci. Technol. B* 1991, 9, 726-9.
- (D190) Yang, Y. N.; Trafas, B. M.; Siefert, R. L.; Weaver, J. H. *Phys. Rev. B* 1991, 44, 3218-21.
- (D191) Bonnell, D. A.; Rohrer, G. S.; French, R. H. *J. Vac. Sci. Technol. B* 1991, 9, 551-6.
- (D192) Rohrer, G. S.; Bonnell, D. A. *J. Vac. Sci. Technol. B* 1991, 9, 783-8.
- (D193) Rohrer, G.; Bonnell, D. A. *Surf. Sci.* 1991, 247, L195-200.
- (D194) Stocker, W.; Magdonov, S. N.; Cantow, H. J.; Boettner, H.; Scheib, S.; Melscher, M.; Take, M. *Fresenius J. Anal. Chem.* 1991, 341, 184-8.
- (D195) Focke, T.; King, R.; Dale, A.; Gerberich, W. W. *Mater. Res. Soc. Symp. Proc.* 1991, 209, 617-22.
- (D196) Rohrer, G.; Bonnell, D. A. *NIST Spec. Publ.* 1991, 804, 447-54.
- (D197) Kashiyawa, S.; Koyanagi, M.; Shoji, A.; Matsuda, M.; Shibata, H. *IEEE Trans. Magn.* 1991, 27, 837-9.
- (D198) Kashiyawa, S.; Koyanagi, M.; Shoji, A.; Matsuda, M.; Shibata, H.; Hajima, K. *Physica B* 1991, 169, 485-6.
- (D199) Inoue, K.; Takayanagi, H. *Phys. Rev. B* 1991, 43, 6214-5.
- (D200) Thomsson, S. L.; Murdock, J. M.; Chan, H. *IEEE Trans. Magn.* 1991, 27, 3188-91.
- (D201) Chen, T.; Tesmer, S.; Tucker, J. R.; Lyding, J. W.; Van Hartigan, D. *J. Vac. Sci. Technol. B* 1991, 9, 1000-5.
- (D202) Renner, C.; Kant, A. D.; Niedermann, P.; Fischer, O.; Levy, F. *Phys. Rev. Lett.* 1991, 67, 1650-2.
- (D203) Lang, H. P.; Frey, T.; Guentherodt, H. *J. Euphys. Lett.* 1991, 15, 687-70.
- (D204) Jin, S.; Kammlott, G. W.; Nakahara, S.; Tietel, T. H.; Graebner, J. E. *Science* 1991, 253, 427-9.
- (D205) Lovendus, D. H.; Norton, D. P.; Budai, J. D.; Christen, D. K.; Klambund, C. E.; Warmack, R. J.; Pennycook, S. J. *Proc. SPIE—Int. Soc. Opt. Eng.* 1991, 1394, 150-60.
- (D206) Hawley, M.; Reistrick, I. D.; Beery, J. G.; Houston, R. J. *Science* 1991, 251, 1587-9.
- (D207) Krebs, H. U.; Krause, C.; Yang, X.; Geyer, U. *Appl. Phys. Lett.* 1991, 59, 2180-2.
- (D208) Harmer, M. A.; Fincher, C. R.; Parkinson, B. A. *J. Appl. Phys.* 1991, 70, 2760-3.
- (D209) Moreland, J.; Rice, P. *IEEE Trans. Magn.* 1991, 27, 1198-201.
- (D210) Hasegawa, T.; Kikazawa, K. *Bull. Mater. Sci.* 1991, 14, 719-22.
- (D211) Lu, J. X.; Wan, J. C.; Goldman, A. M.; Chang, Y. D.; Jang, P. Z. *Phys. Rev. Lett.* 1991, 67, 2195-8.
- (D212) Terahima, K.; Kondoh, M.; Takamura, Y.; Komaki, H.; Yoshida, T. *Appl. Phys. Lett.* 1991, 59, 644-6.
- (D213) Silver, R. M.; Ogawa, E. T.; Pan, S.; De Lozanne, A. L. *IEEE Trans. Magn.* 1991, 27, 1215-8.
- (D214) Hasegawa, T.; Nantoh, M.; Mochizuki, N.; Kishio, K.; Kikazawa, K. *Supercond. Sci. Technol.* 1991, 4, 873-5.
- (D215) Wu, X. L.; Wang, Y. L.; Zhang, Z.; Lieber, C. M. *Phys. Rev. B* 1991, 43, 8729.
- (D216) Shih, C. K.; Feenstra, R. M.; Chandrasekhar, G. V. *Phys. Rev. B* 1991, 43, 7913-22.
- (D217) Hasegawa, T.; Nantoh, M.; Kikazawa, K. *Jpn. J. Appl. Phys.* 1991, 30, L276-9.
- (D218) Semants, S. B.; Dutta, P. K.; Awana, V. P. S.; Gmelin, E.; Narlikar, A. V. *Physica C* 1991, 178, 171-81.
- (D219) Wang, Y.; Bennema, P.; Schreurs, L. W. M.; Wnuk, J.; Van der Linden, P. *Appl. Phys. A* 1991, 52, 348-52.
- (D220) Parks, D. C.; Wang, J.; Clark, N. A.; Hermann, A. M. *Appl. Phys. Lett.* 1991, 59, 1506-8.
- (D221) Zhang, Z.; Lieber, C. M.; Ginley, D. S.; Baughman, R. J.; Morosin, B. *J. Vac. Sci. Technol. B* 1991, 9, 1009-12.
- (D222) Parkinson, B. A.; Ohuchi, F. S.; Ueno, K.; Koma, A. *Appl. Phys. Lett.* 1991, 58, 472-4.
- (D223) Ohuchi, F. S.; Shimada, T.; Parkinson, B. A.; Ueno, K.; Koma, A. *J. Cryst. Growth* 1991, 111, 1033-7.
- (D224) Heckl, W. M.; Ohnesorge, F.; Binnig, G.; Specht, M.; Hashmi, M. *J. Vac. Sci. Technol. B* 1991, 9, 1072-80.
- (D225) Youngquist, M. G.; Baldeeschweiler, J. D. *J. Vac. Sci. Technol. B* 1991, 9, 1083-7.
- (D226) Parkinson, B. A.; Ren, J.; Whangbo, M. H. *J. Am. Chem. Soc.* 1991, 113, 7833-7.
- (D227) Wu, X. L.; Lieber, C. M. *J. Vac. Sci. Technol. B* 1991, 9, 1044-7.
- (D228) Slough, C. G.; McNairy, W. W.; Wang, C.; Coleman, R. V. *J. Vac. Sci. Technol. B* 1991, 9, 1036-8.
- (D229) Burk, B.; Thomson, R. E.; Zetti, A.; Clarke, J. *Phys. Rev. Lett.* 1991, 66, 3040-3.
- (D230) Dai, H.; Chen, H.; Lieber, C. M. *Phys. Rev. Lett.* 1991, 66, 3183-6.
- (D231) Sakamaki, K.; Fujishima, A.; Onuki, Y. *J. Phys. Chem. Solids* 1991, 52, 409-18.
- (D232) Gammels, J.; Gould, S. A. C.; Hanama, P. K.; Coleman, R. V. *J. Vac. Sci. Technol. B* 1991, 9, 1032-5.
- (D233) Reina, G.; Sattler, K.; Muller, U.; Venkateswaran, N.; Xie, J. *J. Vac. Sci. Technol. B* 1991, 9, 1039-43.
- (D234) Gammels, J.; Hubacek, J. S.; Skala, S. L.; Tucker, J. R.; Lyding, J. W. *J. Vac. Sci. Technol. B* 1991, 9, 1027-31.
- (D235) Dai, Z.; Slough, C. G.; Coleman, R. V. *Phys. Rev. Lett.* 1991, 66, 1318-21.
- (D236) Van Smaalen, S.; De Boer, J. L.; Coppens, P.; Graafma, H. *Phys. Rev. Lett.* 1991, 67, 1471.
- (D237) Dai, Z.; Slough, C. G.; Coleman, R. V. *Phys. Rev. Lett.* 1991, 67, 1472.
- (D238) Wang, C.; Slough, C. G.; Coleman, R. V. *J. Vac. Sci. Technol. B* 1991, 9, 1048-51.
- (D239) Akari, S.; Moeller, R.; Dransfeld, K. *Appl. Phys. Lett.* 1991, 58, 243-5.
- (D240) Van Bekel, G. P. E. M.; De Hoonen, J. T. M.; Hibma, T. *Mater. Res. Soc. Symp. Proc.* 1991, 209, 605-10.
- (D241) Sautys, D.; Rudd, G.; Garfunkel, E. *J. Appl. Phys.* 1991, 69, 1707-11.
- (D242) Rudd, G.; Novak, D.; Sautys, D.; Bertynski, R. A.; Garofalini, S.; Ramaniujachary, K. V.; Greenblatt, M.; Garfunkel, E. *J. Vac. Sci. Technol. B* 1991, 9, 909-13.
- (D243) Clemmer, C. R.; Beebe, T. P., Jr. *Science* 1991, 251, 640-2.
- (D244) Chang, H.; Bard, A. J. *Langmuir* 1991, 7, 1143-53.
- (D245) Siperko, L. M. *J. Vac. Sci. Technol. B* 1991, 9, 1061-3.
- (D246) Liu, C. Y.; Chang, H.; Bard, A. J. *Langmuir* 1991, 7, 1138-42.
- (D247) Sawamura, M.; Womeladorf, J. F.; Ermer, W. C. *J. Phys. Chem.* 1991, 95, 8823-6.
- (D248) Buckley, J. E.; Wrapp, J. L.; White, H. W.; Bruckdorfer, A.; Worcester, D. L. *J. Vac. Sci. Technol. B* 1991, 9, 1079-82.
- (D249) Oden, P. I.; Thundat, T.; Nagahara, L. A.; Lindsey, S. M.; Adams, G. B.; Sarkey, O. F. *Surf. Sci.* 1991, 254, L454-9.
- (D250) Myrick, M. L.; Hud, N. V.; Angel, S. M.; Garvia, D. G. *Chem. Phys. Lett.* 1991, 180, 158-60.
- (D251) Brown, N. M. D.; You, H. X. *J. Mater. Chem.* 1991, 1, 469-72.
- (D252) Ok, C. H.; Heremans, J.; Dreesehaus, M. S.; Speck, J. S.; Nichols, J. T. *J. Vac. Sci. Technol. B* 1991, 9, 1055-60.
- (D253) Kelly, S. P.; Lieber, C. M. *J. Vac. Sci. Technol. B* 1991, 9, 1068-71.
- (D254) Kelly, S. P.; Lu, Z.; Lieber, C. M. *Phys. Rev. B* 1991, 44, 4064-7.
- (D255) Yamazaki, S.; Tanaka, M.; Tanaka, S.; Fughami, M.; Uemori, R.; Fujita, D.; Horino, T.; Ono, M. *J. Vac. Sci. Technol. B* 1991, 9, 883-5.
- (D256) Itoh, H.; Ichinose, T.; Oshima, C.; Ichinokawa, T.; Aizawa, T. *Surf. Sci.* 1991, 254, L437-42.
- (D257) Murata, K.; Yumura, M.; Ueda, H.; Nozoe, H.; Kawabata, Y. *J. Chem. Soc., Chem. Commun.* 1991, 1387-8.
- (D258) Ito, K.; Yonemitsu, T.; Etoh, K.; Sekiguchi, H.; Yamada, I.; Kataoka, H.; Durand, H. A. *Nucl. Instrum. Methods Phys. Res.* 1991, B50-60, 321-5.
- (D259) Vandenop, G. J.; Nascenzo, P. A. P.; Kawasaki, M.; Ogletree, D. F.; Somorjai, G. A.; Selmeron, M. *J. Vac. Sci. Technol. A* 1991, 9, 2273-8.
- (D260) Turner, K. F.; Stoner, B. R.; Bergman, L.; Glass, J. T.; Nemanich, R. J. *J. Appl. Phys.* 1991, 69, 6400-5.
- (D261) Phelps, A. W.; Owens, T. W. *Proc. Electrochem. Soc.* 1991, 91, 502-9.
- (D262) Everson, M. P.; Tamor, M. A. *J. Vac. Sci. Technol. B* 1991, 9, 1570-8.
- (D263) Tsuno, T.; Imai, T.; Nishibayashi, Y.; Hamada, K.; Fujimori, N. *Jpn. J. Appl. Phys.* 1991, 30, 1063-6.
- (D264) Ferrer, S.; Comin, F.; Martin, J. A.; Vazquez, L.; Bernard, P. *Surf. Sci.* 1991, 251-252, 940-4.
- (D265) Busmann, H. G.; Sprang, H.; Harter, I. V.; Zimmermann-Edling, W.; Guentherodt, H. *J. Appl. Phys. Lett.* 1991, 59, 295-7.
- (D266) Collins, C. B.; Davantoo, F.; Jander, D. R.; Lee, T. J.; Park, H.; You, J. H. *J. Appl. Phys.* 1991, 69, 7862-70.
- (D267) Tuner, K. F.; LaGrice, Y. M.; Stoner, B. R.; Glass, J. T.; Nemanich, R. J. *J. Vac. Sci. Technol. B* 1991, 9, 914-8.
- (D268) Funamoto, H.; Kosaki, O.; Sugita, T. *Surf. Coat. Technol.* 1991, 47, 474-80.
- (D269) Ekund, E. A.; Bruhema, R.; Rudnick, J.; Williams, R. S. *Phys. Rev. Lett.* 1991, 67, 1759-62.
- (D270) Kemmer, H.; Grafstrom, S.; Angert, N.; Neumann, R.; Trautmann, C.; Vetter, J. *GSI-Rep.* 1991, 91, 248.
- (D271) Shedd, G. M.; Russell, P. E. *J. Vac. Sci. Technol. A* 1991, 9, 1281-4.

## MICROSCOPY

- (D271) Porte, L.; De Willemeuve, C. H.; Phaner, M. *J. Vac. Sci. Technol. A* 1991, 9, 1064-7.
- (D272) Shen, T. C.; Brockenbrough, R. T.; Hubacek, J. S.; Tucker, J. R.; Lyding, J. W. *J. Vac. Sci. Technol. A* 1991, 9, 1376-9.
- (D273) Buchholz, S.; Fuchs, H.; Rabe, J. P. *Adv. Mater.* 1991, 3, 51-4.
- (D274) Penner, R. M.; Heben, M. J.; Lewis, N. S.; Quate, C. F. *Appl. Phys. Lett.* 1991, 58, 1369-91.
- (D275) Robinson, R. S.; Sternitzke, K.; McCreery, R. L. *J. Vac. Sci. Technol. A* 1991, 9, 990-3.
- (D276) Robinson, R. S.; Sternitzke, K.; McDermott, M. T.; McCreery, R. L. *J. Electrochem. Soc.* 1991, 138, 2412-8.
- (D277) Balooch, M.; Schildbach, M.; Tench, R.; Allen, M.; Siekhaus, W. J. *J. Vac. Sci. Technol. A* 1991, 9, 1088-91.
- (D278) Freund, M. S.; Braiter-Toth, A.; Cotton, T. M.; Henderson, E. R. *Anal. Chem.* 1991, 63, 1047-9.
- (D279) Chang, H.; Bard, A. J. *J. Am. Chem. Soc.* 1991, 113, 5588-96.
- (D280) Hoffman, W. P.; Hurley, W. C.; Liu, P. M.; Owens, T. W. *J. Mater. Res.* 1991, 6, 1685-94.
- (D281) Hoffman, W. P.; Hurley, W. C.; Owens, T. W.; Phan, H. T. *J. Mater. Sci.* 1991, 26, 4545-53.
- (D282) Eigler, D. M.; Weiss, P. S.; Schweizer, E. K.; Lang, N. D. *Phys. Rev. Lett.* 1991, 66, 1189-92.
- (D283) Eigler, D. M.; Lutz, C. P.; Rudge, W. E. *Nature (London)* 1991, 352, 600-3.
- (D284) Whitman, L. J.; Strosio, J. A.; Dragoset, R. A.; Celotta, R. J. *Science* 1991, 251, 1206-10.
- (D285) Hallmark, V. M.; Chiang, S.; Brown, J. K.; Wolf, C. *Phys. Rev. Lett.* 1991, 66, 48-51.
- (D286) Magonov, S. N.; Cantow, H. J.; Van den Ham, D. M. W. *Synth. Met.* 1991, 42, 2639-42.
- (D287) Ruan, L.; Bai, C.; Wang, H.; Hu, Z.; Wan, M. *J. Vac. Sci. Technol. B* 1991, 9, 1134-6.
- (D288) Neijoh, H. *Nature (London)* 1991, 353, 640-2.
- (D289) Zippel, E.; Breiter, M. W.; Kellner, R. *J. Chem. Soc., Faraday Trans* 1991, 87, 637-42.
- (D290) Tesar, A. A.; Balooch, M.; Shortt, K. W.; Siekhaus, W. J. *Proc. SPIE—Int. Soc. Opt. Eng.* 1991, 1441, 228-36.
- (D291) Marrion, C. R. K.; Dobiaz, E. A.; Colton, R. J. *J. Vac. Sci. Technol. B* 1991, 9, 1367-70.
- (D292) Magonov, S. N.; Ovarstrom, K.; Huang, D. M.; Elings, V.; Cantow, H. *J. Polym. Mater. Sci. Eng.* 1991, 65, 163-4.
- (D293) Magonov, S. N.; Ovarstrom, K.; Elings, V.; Cantow, H. *J. Polym. Bull. (Berlin)* 1991, 25, 669-94.
- (D294) Yang, A. C. M.; Tarris, B. D.; Kunz, M. *Macromolecules* 1991, 24, 6800-2.
- (D295) Zhai, P.; Tang, X.; Bai, C.; Zhao, J.; Gu, J.; Vetter, J.; Spohr, R. *GSI-Rep.* 1991, 97, 248.
- (D296) Lee, E. H.; Lewis, M. B.; Blau, P. J.; Mansur, L. K. *J. Mater. Res.* 1991, 6, 610-28.
- (D297) Srinam, T. S.; Wahi, K. J.; Chung, Y. W.; Bhushan, B.; Rothchild, W. *J. Tribol.* 1991, 113, 245-9.
- (D298) Lotz, B.; Wittmann, J. C.; Stocker, W.; Magonov, S. N.; Cantow, H. *J. Polym. Bull. (Berlin)* 1991, 26, 209-14.
- (D299) Yang, R.; Yang, X. R.; Evans, D. F.; Hendrickson, W. A.; Baker, J. *J. Phys. Chem.* 1991, 95, 3765-7.
- (D300) Mate, C. M.; Novotny, V. *J. Chem. Phys.* 1991, 94, 8420-7.
- (D301) Dietz, P.; Hanama, P. K.; Herrmann, K. H.; Inacker, O.; Lehmann, H. D. *Ultramicroscopy* 1991, 35, 155-9.
- (D302) MacKay, S. G.; Bakir, M.; Musselman, I. H.; Meyer, T. J.; Linton, R. W. *Anal. Chem.* 1991, 63, 60-5.
- (D303) Madson, L. L.; Carneiro, K.; Zaba, B. N.; Underhill, A. E.; Van der Stuij, M. *J. Synth. Met.* 1991, 43, 2631-4.
- (D304) Everson, M. P.; Helms, J. H. *Synth. Met.* 1991, 40, 97-109.
- (D305) Porter, T. L.; Dillingham, T. R.; Lee, C. Y.; Jones, T. A.; Wheeler, B. L.; Caple, G. *Synth. Met.* 1991, 40, 187-96.
- (D306) Porter, T. L.; Lee, C. Y.; Wheeler, B. L.; Caple, G. *J. Vac. Sci. Technol. B* 1991, 9, 1462-8.
- (D307) Jeon, D.; Kim, J.; Gallagher, M. C.; Wills, R. F.; Kim, Y. T. *J. Vac. Sci. Technol. B* 1991, 9, 1164.
- (D308) Armas, S. P.; Alizal, M.; Hawley, M.; Beery, J. G.; Gottesfeld, S. *Langmuir* 1991, 7, 1447-52.
- (D309) Armas, S. P.; Gottesfeld, S.; Beery, J. G.; Garzon, F.; Mombourquette, C.; Hawley, M.; Kuhn, H. H. *J. Mater. Chem.* 1991, 1, 525-9.
- (D310) Karvava, S. J.; Zagorska, M.; Driehs, B.; Soederholm, S. *Phys. Ser.* 1991, 44, 112-5.
- (D311) Mizes, H. A.; Loh, K. G.; Miller, R. J. D.; Corwell, E. M.; Arbuckle, G. A.; Theophilou, N.; Macfarland, A. G.; Hsieh, B. R. *Mol. Cryst. Liq. Cryst.* 1991, 194, 305-10.
- (D312) Fuchs, H.; Eng, L. M.; Sander, R.; Petermann, J.; Jendr, K. D.; Hoffmann, T. *Polym. Bull. (Berlin)* 1991, 26, 95-100.
- (D313) Oka, Y.; Takahashi, A. *Polym. J. (Tokyo)* 1991, 23, 805-8.
- (D314) Wang, J.; Martinez, T.; Yaniv, D. R.; McCormick, L. D. *J. Electroanal. Chem. Interfacial Electrochem.* 1991, 313, 129-40.
- (D315) Yang, R.; Neol, K.; Evans, D. F.; Smyrl, W. H.; Hendrickson, W. A. *Langmuir* 1991, 7, 566-8.
- (D316) Iwakabe, Y.; Hara, M.; Kondo, K.; Tochigi, K.; Mukoh, A.; Yamada, A.; Garito, A. F.; Sasabe, H. *Jpn. J. Appl. Phys.* 1991, 30, 2542-60.
- (D317) Shigano, M.; Ohmi, M.; Sugino, M.; Mizutani, W. *Mol. Cryst. Liq. Cryst.* 1991, 199, 141-9.
- (D318) Brandow, S. L.; DiLolla, D. P.; Cotton, R. J.; Shaahidhar, R. *J. Vac. Sci. Technol. B* 1991, 9, 1115-8.
- (D319) Mizutani, W.; Shigano, M.; Sugino, M.; Kajimura, K.; Ono, M. *J. Vac. Sci. Technol. B* 1991, 9, 1102-6.
- (D320) McMaster, T. J.; Carr, H.; Miles, M. J.; Cairns, P.; Morris, V. *J. Liq. Cryst.* 1991, 9, 11-8.
- (D321) Smith, D. P. E. *J. Vac. Sci. Technol. B* 1991, 9, 1119-25.
- (D322) Neijoh, H. *Surf. Sci.* 1991, 256, 94-101.
- (D323) Wang, Z.; Zhang, P.; Moskovits, M. *Mater. Res. Soc. Symp. Proc.* 1991, 206, 709-13.
- (D324) Chen, T.; Howells, S.; Gallagher, M.; Yi, L.; Sand, D.; Lichtenberger, D. L.; Nebesny, K. W.; Ray, C. D. *J. Vac. Sci. Technol. B* 1991, 9, 2461-5.
- (D325) Li, Y. Z.; Pattn, J. C.; Chander, M.; Weaver, J. H.; Chibante, L. P. F.; Smalley, R. E. *Science* 1991, 252, 547-8.
- (D326) Li, Y. Z.; Chander, M.; Pattn, J. C.; Weaver, J. H.; Chibante, L. P. F.; Smalley, R. E. *Science* 1991, 253, 429-33.
- (D327) Snyder, E. J.; Anderson, M. S.; Tong, W. M.; Williams, R. S.; Anz, S. J.; Alvarez, M. M.; Rubin, Y.; Diederich, F. N.; Whetten, R. L. *Science* 1991, 253, 171-3.
- (D328) Leung, M. S.; Ives, N. A.; Stupien, G. W. *J. Appl. Phys.* 1991, 69, 2044-7.
- (D329) Hawley, M. E.; Benicewicz, B. C. *J. Vac. Sci. Technol. B* 1991, 9, 1141-7.
- (D330) Fujiwara, I.; Ishimoto, C.; Seto, J. *J. Vac. Sci. Technol. B* 1991, 9, 1148-53.
- (D331) Hanama, H. G.; Gould, S. A. C.; Hanama, P. K.; Gaub, H. E.; Longo, M. L.; Zasadzinski, J. A. N. *Langmuir* 1991, 7, 1051-4.
- (D332) Bourdieu, L.; Silberzan, P.; Chatenay, D. *Phys. Rev. Lett.* 1991, 67, 2029-32.
- (D333) Meyer, E.; Howald, L.; Overney, R. M.; Henzelmann, H.; Frommer, J.; Guentheroth, H. J.; Wagner, T.; Scher, H.; Roth, S. *Nature* 1991, 349, 398-400.
- (D334) Weisenhorn, A. L.; Egger, M.; Ohnesorge, F.; Gould, S. A. C.; Heyn, S. P.; Hanama, H. G.; Sinsheimer, R. L.; Gaub, H. E.; Hanama, P. K. *Langmuir* 1991, 7, 8-12.
- (D335) Yang, J.; Takeyasu, K.; Somiya, A. P.; Shao, Z. *FEBS Lett.* 1991, 279, 295-9.
- (D336) McMaster, T. J.; Carr, H. J.; Miles, M. J.; Cairns, P.; Morris, V. *J. Macromolecules* 1991, 24, 1428-30.
- (D337) Shigakawa, H.; Morozumi, T.; Komyama, M.; Yoshimura, M.; Kawazu, A.; Saito, Y. *J. Vac. Sci. Technol. B* 1991, 9, 1189-92.
- (D338) Heckl, W. M.; Smith, D. P. E. *J. Vac. Sci. Technol. B* 1991, 9, 1159-61.
- (D339) Vandenberg, E. T.; Bertleson, L.; Lidberg, B.; Uvdal, K.; Erlendsson, R.; Elving, H.; Lundstrom, I. *J. Colloid Interface Sci.* 1991, 147, 103-16.
- (D340) Dawson, P.; Haas, J. W., III; Alexander, K. B.; Thompson, J.; Ferrel, T. L. *Surf. Sci.* 1991, 250, L383-8.
- (D341) Rabe, J. P.; Buchholz, S. *Science* 1991, 253, 424-7.
- (D342) McGonigal, G. C.; Bernhardt, R. H.; Yeo, Y. H.; Thomson, D. J. *J. Vac. Sci. Technol. B* 1991, 9, 1107-10.
- (D343) Armstrong, M. J.; Muller, R. H. *J. Electrochem. Soc.* 1991, 138, 2303-7.
- (D344) Kuroda, R.; Kishi, E.; Yamano, A.; Hatanaka, K.; Matsuda, H.; Eguchi, K.; Nakagiri, T. *J. Vac. Sci. Technol. B* 1991, 9, 1180-3.
- (D345) Rabe, J. P.; Buchholz, S. *Phys. Rev. Lett.* 1991, 66, 2096-9.
- (D346) Stocker, W.; Bar, G.; Kunz, M.; Moeller, M.; Magonov, S. N.; Cantow, H. *J. Polym. Bull. (Berlin)* 1991, 26, 215-22.
- (D347) Widrig, C. A.; Alvas, C. A.; Porter, M. C. *J. Am. Chem. Soc.* 1991, 113, 2806-10.
- (D348) Sun, L.; Crooks, R. M. *J. Electrochem. Soc.* 1991, 138, L23-5.
- (D349) Kekoven, B. M.; Meyers, G. F. *J. Vac. Sci. Technol. A* 1991, 9, 2570-7.
- (D350) Kelta, B.; Nadjo, L. *Surf. Sci.* 1991, 254, L443-7.
- (D351) Weinrach, J. B.; Hawley, M.; Sattelberger, A. P.; Swanson, B. I. *Solid State Commun.* 1991, 77, 653-8.
- (D352) Li, Y.; Lindsay, S. M. *Rev. Sci. Instrum.* 1991, 62, 2630-3.
- (D353) Dotan, C.; Yuan, Y.; Jao, T. C.; Fendler, J. H. *Chem. Mater.* 1991, 3, 215-8.
- (D354) Lindgreen, H.; Garnaes, J.; Hansen, P. L.; Beenenbacher, F.; Laegaard, E.; Stenegaard, I. v.; Gould, S. A. C.; Hanama, P. K. *Am. Mineral.* 1991, 76, 1218-22.
- (D355) Rauf, I. A.; Walls, M. G. *Ultramicroscopy* 1991, 35, 19-26.
- (D356) Magonov, S. N.; Kempf, S.; Schuchardt, J.; Bar, G.; Gronski, W.; Cantow, H. *J. Synth. Met.* 1991, 42, 1815-8.
- (D357) Kosemehl, G.; Kabbeck-Kupfai, D.; Magonov, S. N. *Synth. Met.* 1991, 42, 2565-8.
- (D358) Matsumoto, M.; Nishio, Y.; Tachibana, H.; Nakamura, T.; Kawabata, Y.; Samura, H.; Nagamura, T. *Chem. Lett.* 1991, 6, 1021-4.
- (D359) Yamaguchi, S.; Vianda, C. A.; Potember, R. S. *J. Vac. Sci. Technol. B* 1991, 9, 1129-33.
- (D360) Magonov, S. N.; Schuchardt, J.; Kempf, S.; Keller, E.; Cantow, H. *J. Synth. Met.* 1991, 40, 59-72.
- (D361) Magonov, S. N.; Kempf, S.; Rottler, H.; Cantow, H. *J. Synth. Met.* 1991, 40, 73-86.
- (D362) Pan, S.; De Lozanne, A. L.; Falchheim, R. *J. Vac. Sci. Technol. B* 1991, 9, 1017-21.
- (D363) Yoshimura, M.; Shigakawa, H.; Yamochi, H.; Saito, G.; Saito, Y.; Kawazu, A. *Phys. Rev. B* 1991, 44, 1970-2.
- (D364) Magonov, S. N.; Bar, G.; Keller, E.; Yagubskii, E. B.; Cantow, H. *J. Synth. Met.* 1991, 40, 247-56.
- (D365) Miura, Y. F.; Kasai, A.; Nakamura, T.; Komizu, H.; Matsumoto, M.; Kawabata, Y. *Mol. Cryst. Liq. Cryst.* 1991, 196, 161-5.
- (D366) Yoshimura, M.; Shigakawa, H.; Neijoh, H.; Saito, G.; Saito, Y.; Kawazu, A. *Phys. Rev. B* 1991, 43, 13590-3.
- (D367) Mori, Y.; Maruyama, Y.; Mori, H.; Saito, G. *Jpn. J. Appl. Phys.* 1991, 30, L358-60.
- (D368) Yoshimura, M.; Ara, N.; Kagoshima, M.; Shiota, R.; Kawazu, A.; Shigakawa, H.; Saito, Y.; Oshima, M.; Mori, H. *Surf. Sci.* 1991, 242, 18-22.
- (D369) Kawazu, A.; Yoshimura, M.; Shigakawa, H.; Mori, H.; Saito, G. *J. Vac. Sci. Technol. B* 1991, 9, 1006-8.

- (D370) Feinchen, R.; Murphy, J. C. *J. Vac. Sci. Technol. B* 1991, 9, 1013-6.
- (D371) Overmyer, R. M.; Howald, L.; Frommer, J.; Meyer, E.; Guentherodt, H. *J. Chem. Phys.* 1991, 94, 8441-3.
- (D372) Bar, G.; Magonov, S. N.; Cantow, H. J.; Dietrich, M.; Heinze, J. *Synth. Met.* 1991, 42, 2335-8.
- (D373) Magonov, S. N.; Bar, G.; Cantow, H. J.; Gauer, H. D.; Mueller, I.; Schworer, M. *Polym. Bull.* (Berlin) 1991, 26, 223-30.
- (D374) Gratz, A. J.; Manne, S.; Hanama, P. K. *Science* 1991, 251, 1343-8.
- (D375) Shindo, H.; Kase, M.; Kondoh, H.; Nishihara, C.; Hayakawa, H.; Ono, S.; Nozoye, H. *J. Chem. Soc., Chem. Commun.* 1991, 1097-9.
- (D376) Thibaudau, F.; Cousty, J.; Balazat, E.; Bouffard, S. *Phys. Rev. Lett.* 1991, 67, 1582-5.
- (D377) Jansen, J. C.; Schoonman, J.; Van Bekum, H.; Pinet, V. *Zoolites* 1991, 11, 306-7.
- (D378) MacDougall, J. E.; Cox, S. D.; Stucky, G. D.; Weisenhorn, A. L.; Hanama, P. K.; Wise, W. S. *Zoolites* 1991, 11, 426-33.
- (D379) Meyer, E.; Guentherodt, H. J.; Haefke, H.; Garth, G.; Krohn, M. *Europhys. Lett.* 1991, 15, 319-23.
- (D380) Haefke, H.; Meyer, E.; Guentherodt, H. J.; Garth, G.; Krohn, M. *J. Imaging Sci.* 1991, 35, 290-2.
- (D381) Ketta, B.; Nadjio, L.; Kjofer, K. *Surf. Sci.* 1991, 259, L613-7.
- (D382) Masaki, N.; Masuda, K.; Kado, H.; Yokoyama, K.; Tohda, T. *Chem. Pharm. Bull.* 1991, 39, 1899-901.
- (D383) Slawka-Waniewska, A.; Slomko, A.; Sertozo, G. *J. Magn. Mater.* 1991, 93, 169-73.
- (D384) Fukumoto, H.; Hamada, T.; Endo, T.; Osaka, Y. *J. Appl. Phys.* 1991, 69, 8076-8.
- (D385) Thompson, M.; Ellings, V. *Am. Lab. (Fairfield, Conn.)* 1991, 23, 36.
- (D386) Wilson, T. E.; Murray, M. N.; Ogletree, D. F.; Bednarik, M. D.; Cantow, C. R.; Salmeron, M. B. *J. Vac. Sci. Technol. B* 1991, 9, 1171-8.
- (D387) Mou, J.; Sun, W.; Yan, J.; Yang, W. S.; Liu, C.; Zhai, Z.; Xu, Q.; Xie, Y. *J. Vac. Sci. Technol. B* 1991, 9, 1566-9.
- (D388) Sasebe, H.; Furuno, T.; Otomo, J.; Sato, A.; Nagamura, T.; Umer, K. *M. New J. Chem.* 1991, 15, 149-52.
- (D389) Kolomytskiy, O. V.; Golubok, A. O.; Davydov, D. N.; Timofeev, V. A.; Vinogradova, S. A.; Tiplav, S. Ya. *Biophys. J.* 1991, 59, 889-93.
- (D390) Leatherbarrow, R. J.; Stadman, M.; Wells, T. N. C. *J. Mol. Biol.* 1991, 227, 361-5.
- (D391) Ok, C. H.; Harems, J.; Lee, P. S.; Oziedzic, D.; Sargent, N. E. *J. Vac. Sci. Technol. B* 1991, 9, 1266-71.
- (D392) Edstrom, R. D.; Miller, M. A.; Ellings, V. B.; Yang, X.; Yang, R.; Lee, G.; Evans, D. F. *J. Vac. Sci. Technol. B* 1991, 9, 1248-52.
- (D393) Lee, G.; Evans, D. F.; Ellings, V.; Edstrom, R. D. *J. Vac. Sci. Technol. B* 1991, 9, 1236-41.
- (D394) Miwa, T.; Kobatake, E.; Ikariyama, Y.; Aizawa, M. *Bioconjugate Chem.* 1991, 2, 270-4.
- (D395) Vernell, L. A.; Nowlin, C. L. A.; Hamaroff, S. R.; Gandolfi, A. J.; Lee, Y. C.; Serid, D. *J. Vac. Sci. Technol. B* 1991, 9, 1223-6.
- (D396) Haggerty, L.; Watson, B. A.; Barbeau, M. A.; Lenthof, A. M. *J. Vac. Sci. Technol. B* 1991, 9, 1119-22.
- (D397) Pizzoloni, V.; Page, D. *Polym. Prepr. (Am. Chem. Soc., Div. Polym. Chem.)* 1991, 32, 229.
- (D398) Yeung, K. L.; Wolf, E. E.; Duman, J. G. *J. Vac. Sci. Technol. B* 1991, 9, 1197-201.
- (D399) Amrein, M.; Wang, Z.; Guckenberger, R. *J. Vac. Sci. Technol. B* 1991, 9, 1276-81.
- (D400) Zhu, X. Y.; Poirier, G. E.; White, J. M. *J. Vac. Sci. Technol. A* 1991, 9, 179-81.
- (D401) Miles, M. J.; Carr, H. J.; McMaster, T. C.; l'Anson, K. J.; Bolton, P. S.; Morris, V. J.; Field, J. M.; Shawry, P. R.; Tatham, A. S. *Proc. Natl. Acad. Sci. U.S.A.* 1991, 88, 66-71.
- (D402) Masaki, J.; Shibata, T.; Kondo, S.; Ishiwata, S. *J. Vac. Sci. Technol. B* 1991, 9, 1177-9.
- (D403) Hackl, W. M.; Smith, D. P. E.; Binnig, G.; Klages, H.; Haensch, T. W.; Maddocks, J. *Proc. Natl. Acad. Sci. U.S.A.* 1991, 88, 8003-6.
- (D404) Leontiewska, E.; Pawtan, P. J.; Cechla, C.; Schreiber, J. P.; Gaudonnet, J. P. *Biochem. Biophys. Res. Commun.* 1991, 178, 1280-7.
- (D405) Keller, R. W.; Bear, D.; Bustamante, C. *J. Vac. Sci. Technol. B* 1991, 9, 1291-7.
- (D406) Lindsay, S. M.; Philipp, M. *Geset. Anal. Tech. Appl.* 1991, 9, 8-13.
- (D407) De Stasio, G.; Ribuz, D.; Margaritondo, G.; Mercanti, D.; Trassetti, L.; Moore, C. *J. Vac. Sci. Technol. B* 1991, 9, 2319-21.
- (D408) Youngquist, M. G.; Orlicoll, R. J.; Coley, T. R.; Goddard, W. A.; Biederman, J. D. *J. Vac. Sci. Technol. B* 1991, 9, 1304-8.
- (D409) Saito, S.; Cricenti, A. *Phys. Scr.* 1991, 73F, 107-10.
- (D410) Cricenti, A.; Saito, S.; Chiarotti, G.; Arnold, F. *J. Vac. Sci. Technol. B* 1991, 9, 1296-7.
- (D411) Lyubchenko, Y. L.; Lindsay, S. M.; DeRose, J. A.; Thundat, T. *J. Vac. Sci. Technol. B* 1991, 9, 1288-90.
- (D412) Bai, C.; Yie, J.; Gong, L.; Dai, C.; Wang, D.; Gao, F.; Gu, J. *Chin. Sci. Bull.* 1991, 36, 345-7.
- (D413) Li, Mingqian; Zhu, J.; Zhu, J.; Hu, J.; Gu, M.; Xu, Y.; Zhang, L.; Huang, Z.; Xu, L.; Yao, X. *J. Vac. Sci. Technol. B* 1991, 9, 1296-303.
- (D414) Allan, M. J.; Tench, R. J.; Mazzimas, J. A.; Balooch, M.; Stekhaus, W. J.; Beham, R. *J. Vac. Sci. Technol. B* 1991, 9, 1272-5.
- (D415) Lindsay, S. M.; Li, Y.; Pan, J.; Thundat, T.; Nagahara, L. A.; Oden, P.; DeRose, J. A.; Knipping, U.; White, J. W. *J. Vac. Sci. Technol. B* 1991, 9, 1099-101.
- (D416) DeRose, J. A.; Lindsay, S. M.; Nagahara, L. A.; Oden, P. I.; Thundat, T.; Hill, R. L. *J. Vac. Sci. Technol. B* 1991, 9, 1189-70.
- (D417) Hanama, H. G.; Weisenhorn, A. L.; Gould, S. A. C.; Stahmer, R. L.; Gaub, H. E.; Stucky, G. D.; Zarella, C. M.; Hanama, P. K. *J. Vac. Sci. Technol. B* 1991, 9, 1292-4.
- (D418) Friedbacher, G.; Hanama, P. K.; Ramil, E.; Stucky, G. D. *Science* 1991, 253, 1261-3.
- (D419) Hanama, H. G.; Weisenhorn, A. L.; Edmondson, A. B.; Gaub, H. E.; Hanama, P. K. *Chim. Phys.* 1991, 37, 1497-501.
- (D420) Schmitt, F. J.; Weisenhorn, A. L.; Hanama, P. K.; Knoll, W. *Makromol. Chem., Macromol. Symp.* 1991, 46, 133-43.
- (D421) Wiegraebe, W.; Nonnenmacher, M.; Guckenberger, R.; Wolter, O. *J. Microsc. (Oxford)* 1991, 163, 79-84.
- (D422) Wigren, R.; Ehling, H.; Erlendsson, R.; Welin, S.; Lundstrom, I. *FEBS Lett.* 1991, 280, 225-8.
- (D423) Ferrell, T. L.; Gaudonnet, J. P.; Reddick, R. C.; Sharp, S. L.; Wermack, R. J. *J. Vac. Sci. Technol. B* 1991, 9, 525-30.
- (E1) Ohnori, T.; Hashimoto, K.; Fujishima, A. *Jpn. J. Appl. Phys.* 1991, 30, 1826-9.
- (E2) Roberts, C. J.; Hoffmann-Millock, B.; Steer, W. S. *Surf. Sci.* 1991, 254, L448-53.
- (E3) Hagan, H. P.; Ferguson, A. J. L.; Turner, R. J.; Smith, K. W.; Dawson, P.; Wainman, D. G. *J. Vac. Sci. Technol. B* 1991, 9, 879-82.
- (E4) Salmeron, M.; Ogletree, D. F.; Ocal, C.; Wang, H. C.; Neubauser, G.; Kolbe, W.; Meyers, G. *J. Vac. Sci. Technol. B* 1991, 9, 1347-52.
- (E5) Masegala, S. C.; Reel, F.; Reyes, C. B. *J. Vac. Sci. Technol. B* 1991, 9, 1340-2.
- (E6) Marini, H. J.; Chiang, S.; Birk, H.; Guethner, P. H.; Rugar, D. *J. Vac. Sci. Technol. B* 1991, 9, 1398-402.
- (E7) Hashizume, T.; Hasegawa, Y.; Sumita, I.; Sakurai, T. *Surf. Sci.* 1991, 246, 189-94.
- (E8) Hashizume, T.; Hasegawa, Y.; Sakurai, T. *Appl. Surf. Sci.* 1991, 49-49, 119-24.
- (E9) Hartmann, E.; Behm, R. J.; Krostz, G.; Mueller, G.; Koch, F. *Appl. Phys. Lett.* 1991, 59, 2136-8.
- (E10) Dagata, J. A.; Tseng, W.; Bennett, J.; Schnel, J.; Harary, H. H. *J. Appl. Phys.* 1991, 70, 3661-5.
- (E11) Dagata, J. A.; Schnel, J.; Harary, H. H.; Bennett, J.; Tseng, W. *J. Vac. Sci. Technol. B* 1991, 9, 1384-8.
- (E12) Doblez, E. A.; Martin, C. R. K. *Appl. Phys. Lett.* 1991, 58, 2526-8.
- (E13) Caillias, N.; Snyder, S. R.; White, H. S. *J. Electrochem. Soc.* 1991, 138, 641-2.
- (E14) Fuchs, H.; Schimmel, T. *Adv. Mater. (Weinheim, Fed. Repub. Ger.)* 1991, 3, 112-3.
- (E15) Yau, S. T.; Seltz, D.; Wriekat, A.; Nayfeh, M. H. *J. Appl. Phys.* 1991, 69, 2970-4.
- (E16) Egler, D. M.; Lutz, C. P.; Rudge, W. E. *Nature (London)* 1991, 352, 600-3.
- (E17) Lyo, J. W.; Avouris, P. *Science* 1991, 253, 173-8.
- (F1) Yaniv, D. R.; McCormick, L. D. *Electroanalysis* 1991, 3, 103-10.
- (F2) Michnev, V. A. *Surf. Sci.* 1991, 250, 220-8.
- (F3) Gilbert, S. E. *J. Electrochem. Soc.* 1991, 138, 245C-50C.
- (F4) Horbo, H.; Itaya, K. *J. Chem. Phys.-Chim. Biol.* 1991, 89, 1477-89.
- (F5) Binggall, M.; Carnal, D.; Nyffenegger, R.; Segnerhater, H.; Christoph, R.; Rohrer, H. *J. Vac. Sci. Technol. B* 1991, 9, 1965-82.
- (F6) Trevor, D. J.; Chidsey, C. E. D. *J. Vac. Sci. Technol. B* 1991, 9, 984-8.
- (F7) Holland-Moritz, E.; Gordon, J. II; Kanazawa, K.; Sonnenfeld, R. *Langmuir* 1991, 7, 1961-7.
- (F8) Teo, N. J.; Lindsay, S. M. *J. Appl. Phys.* 1991, 70, 5141-3.
- (F9) Gao, X.; Hamelin, A.; Weaver, M. J. *Phys. Rev. Lett.* 1991, 67, 618-21.
- (F10) Gao, X.; Hamelin, A.; Weaver, M. J. *J. Chem. Phys.* 1991, 95, 6993-6996.
- (F11) McCarty, R. L.; Bard, A. J. *J. Phys. Chem.* 1991, 95, 9618-20.
- (F12) Manne, S.; Masala, J.; Ellings, V. B.; Hanama, P. K.; Gawth, A. A. *J. Vac. Sci. Technol. A* 1991, 9, 950-4.
- (F13) Manne, S.; Hanama, P. K.; Masala, J.; Ellings, V. B.; Gawth, A. A. *Science* 1991, 251, 163-6.
- (F14) Endo, K.; Sugawara, Y.; Mishima, S.; Okada, T.; Morita, S. *Jpn. J. Appl. Phys.* 1991, 30, 2582-3.
- (F15) Oppenheim, I. C.; Trevor, D. J.; Chidsey, C. E. D.; Trevor, P.; Kieradzki, K. *Science* 1991, 254, 687-9.
- (F16) Pickering, H. W.; Wu, Y. C.; Gregory, D. S.; Goh, S.; Sakurai, T. *J. Vac. Sci. Technol. B* 1991, 9, 976-83.
- (F17) Wu, Y. C.; Pickering, H. W.; Gregory, D. S.; Goh, S.; Sakurai, T. *Surf. Sci.* 1991, 246, 468-78.
- (F18) Hopfer, M.; Obresnov, W.; Justine, K.; Lorenz, W. J.; Stakov, G.; Bozhanov, V.; Budevski, E. *Surf. Sci.* 1991, 248, 225-33.
- (F19) Szlarczyk, M.; Bocoris, J. O. *Surf. Sci.* 1991, 241, 54-60.
- (F20) Saitoh, K.; Furuya, N.; Itaya, K. *J. Vac. Sci. Technol. A* 1991, 9, 467-84.
- (F21) Bhardwaj, R. C.; Gonzalez-Martin, A.; Bocoris, J. O. *J. Electrochem. Soc.* 1991, 138, 1901-8.
- (F22) Bhardwaj, R. C.; Gonzalez-Martin, A.; Bocoris, J. O. *J. Electroanal. Chem. Interfacial Electrochem.* 1991, 307, 195-207.
- (F23) Houbertz, R.; Mammert, U.; Behm, R. *J. Appl. Phys. Lett.* 1991, 58, 1027-9.
- (F24) Eriksson, S.; Carlsson, P.; Holmstrom, B.; Uosaki, K. *J. Electroanal. Chem. Interfacial Electrochem.* 1991, 313, 121-8.
- (F25) Zhao, X. K.; McCormick, L.; Fendler, J. H. *Chem. Mater.* 1991, 3, 922-35.
- (F26) Sakamaki, K.; Hinokuma, K.; Fujishima, A. *Collect. Czech. Chem. Commun.* 1991, 56, 104-11.
- (F27) Sakamaki, K.; Hinokuma, K.; Fujishima, A. *J. Vac. Sci. Technol. B* 1991, 9, 944-8.
- (F28) Srinivasan, R.; Murphy, J. C.; Feinchen, R.; Palitabraman, N. *J. Electroanal. Chem. Interfacial Electrochem.* 1991, 312, 293-300.
- (F29) Yau, S. L.; Gao, X.; Cheng, S. C.; Schardt, B. C.; Weaver, M. J. *J. Am. Chem. Soc.* 1991, 113, 6048-66.

- (F30) Vitus, C. M.; Chang, S. C.; Schardt, B. C.; Weaver, M. J. *J. Phys. Chem.* 1991, 95, 7559-63.
- (F31) Chang, S. C.; Yau, S. L.; Schardt, B. C.; Weaver, M. J. *J. Phys. Chem.* 1991, 95, 4787-94.
- (F32) Bard, A. J.; Fan, F.-R.; Pierce, D. T.; Unwin, P. R.; Wipf, D. O.; Zhou, F. *Science* 1991, 68-73.
- (F33) Bard, A. J.; Denault, G.; Friesner, R. A.; Dombleser, B. C.; Tuckerman, L. S. *Anal. Chem.* 1991, 63, 1282-88.
- (F34) Lee, C.; Kwak, J.; Anson, F. C. *Anal. Chem.* 1991, 63, 1301-4.

- (F35) Scott, E. R.; White, H. S.; Phipps, J. B. *J. Membrane Sci.* 1991, 58, 71-87.
- (F36) Yee, S.; Oriani, R. A.; Strathmann, M. *J. Electrochem. Soc.* 1991, 138, 55-61.
- (F37) Hung, S.-M.; Yee, S.; Atarsoold, R. T.; McMillan, C. S.; Oriani, R. A.; Smyrl, W. H. *J. Electrochem. Soc.* 1991, 138, L63-4.
- (F38) Isaacs, H. S. *J. Electrochem. Soc.* 1991, 138, 722-8.
- (F39) Isaacs, H. S.; Deavenport, A. J.; Shipley, A. *J. Electrochem. Soc.* 1991, 138, 390-3.